INDUSTRIAL ENGINEERING MASTER THESIS

Sintering by non-conventional microwave techniques of ferrite-alumina composites

AUTHORESS : Manon PEULTIER

SUPERVISOR : Amparo BORRELL TOMÁS

SUPERVISOR : Rut BENAVENTE MARTÍNEZ

Academic year: 2020-2021

Sintering by non-conventional microwave techniques of ferrite-alumina composites

Acknowledgement

I would like to thank all those who have helped and supported me in this research project at the Universitat Politècnica de València.

First of all, I would like to thank my tutors Borrell Tomás, Amparo and Benavente Martínez, Rut for giving me the opportunity to work on such an interesting subject as the elaboration of ceramics. I would also like to thank them for their listening, their support and above all for all the efforts they have made to enable us to work in the best possible conditions despite this difficult sanitary context.

Secondly, I would like to thank all the people at the Universitat Politècnica de València and the Instituto de Tecnología de Materiales with whom I have had the opportunity to exchange ideas and who have enabled me to make progress in my research.

Finally, I would like to thank my classmates who are also doing a research project in Valencia for their support. In particular, I would like to thank my roommate Audrey Cormery and my friend Antoine Kieffer for their support and motivation, especially when we had to work confined in our houses.

Sintering by non-conventional microwave techniques of ferrite-alumina composites

Resumen

En el presente trabajo fin de máster se pretende estudiar la sinterabilidad de composites de ferrita de Ni-Zn (16 vol%) y alúmina (84 vol%). Para ello han empleado dos técnicas de sinterización diferentes: la sinterización convencional y la sinterización no-convencional por microondas. La sinterización por microondas es una técnica muy prometedora que emplea temperaturas de sinterización más baja, tiempos de procesamiento más cortos y un menor consumo de energía que el convencional. Se estudiarán diferentes parámetros de procesado: temperatura, tiempo y el uso o no de un susceptor.

Las excelentes propiedades de los materiales basados en ferritas Ni-Zn, tales como una alta resistividad eléctrica, alta permeabilidad magnética, alta temperatura de Curie, baja pérdida de potencia, etc., les permiten cubrir una amplia gama de aplicaciones, desde microondas hasta radiofrecuencias, y son importantes tanto desde el punto de vista de la investigación fundamental como de la aplicada: núcleos de transformadores, cabezales de lectura/escritura para cintas digitales de alta velocidad, aplicaciones biomédicas en diagnóstico y terapia…

Finalmente se han analizado las propiedades mecánicas de las muestras obtenidas, además, se han realizado ensayos de: microdureza, observación mediante microscopía óptica y electrónica y difracción de rayos X. Las propiedades eléctricas y magnéticas no se han podido llevar a cabo durante la realización de este proyecto, debido a la actual situación mundial del COVID-19.

Palabras clave: Alúmina, ferrita de Ni-Zn, sinterización por microondas, sinterización convencional, microestructura, propiedades mecánicas.

Resum

En el present treball fi de màster es pretén estudiar la sinterabilitat de composites de ferrita de Ni-Zn (16 vol%) i alúmina (84 vol%). Per a això han emprat dues tècniques de sinterització diferents: la sinterització convencional i la sinterització no-convencional per microones. La sinterització per microones és una tècnica molt prometedora que empra temperatures de sinterització més baixa, temps de processament més curts i un menor consum d'energia que el convencional. S'estudiaran diferents paràmetres de processament: temperatura, temps i l'ús o no d'un susceptor.

Les excel·lents propietats dels materials basats en ferrites Ni-Zn, com ara una alta resistivitat elèctrica, alta permeabilitat magnètica, alta temperatura de Curie, baixa pèrdua de potència, etc., els permeten cobrir una àmplia gamma d'aplicacions, des de microones fins a radiofreqüències, i són importants tant des del punt de vista de la investigació fonamental com de l'aplicada: nuclis de transformadors, capçals de lectura/escriptura per a cintes digitals d'alta velocitat, aplicacions biomèdiques en diagnòstic i teràpia…

Finalment s'han analitzat les propietats mecàniques de les mostres obtingudes, a més, s'han realitzat assajos de: microduresa, observació mitjançant microscòpia òptica i electrònica i difracció de raigs X. Les propietats elèctriques i magnètiques no s'han pogut dur a terme durant la realització d'aquest projecte, a causa de l'actual situació mundial del COVID-19.

Paraules clau: Alúmina, ferrita de Ni-Zn, sinterització per microones, sinterització convencional, microestructura, propietats mecàniques.

Abstract

In the present master's thesis, the sinterability of Ni-Zn ferrite (16 vol%) and alumina (84 vol%) composites is studied. Two different sintering techniques have been used: conventional sintering and non-conventional microwave sintering. Microwave sintering is a very promising technique that uses lower sintering temperatures, shorter processing times and lower energy consumption than conventional sintering. Different processing parameters will be studied: temperature, time, and the use or not of a susceptor.

The excellent properties of materials based on Ni-Zn ferrites, such as high electrical resistivity, high magnetic permeability, high Curie temperature, low power loss, etc., allow them to cover a wide range of applications, from microwaves to radio frequencies, and are important both from the point of view of fundamental and applied research: transformer cores, read/write heads for high-speed digital tapes, biomedical applications in diagnosis and therapy...

Finally, the mechanical properties of the samples obtained have been analyzed. In addition, tests have been carried out on: microhardness, observation by optical and electronic microscopy and X-ray diffraction. The electrical and magnetic properties could not be carried out during the execution of this project, due to the current world situation of the COVID-19.

Keywords: Alumina, Ni-Zn ferrite, microwave sintering, conventional sintering, microstructure, mechanical properties.

Table of contents

List of tables

List of figures

Introduction

Nowadays, ceramics are non-metallic mineral materials with outstanding performance which makes them useful in many industrial sectors as structural or functional elements. These sectors are as various as thinkable: aerospace, medicine, food, industrial and transmission electricity… Due to their heat resistance, they can be used for many tasks for which materials like metals and polymers are unsuitable.

This project will investigate a (Ni-Zn) ferrite-Alumina composite. Nickel-zinc ferrite has high electrical resistivity as well as good magnetic properties, making it a material of choice in low and high frequency applications. This material is, for example, used in antenna rods, power transformers or microwave devices. (Yadoji, Peelamedu, Agrawal, & Roy, 2003) Alumina is known to be an insulator and has good mechanical properties. (Croquesel, 2015)

It is well known that the shaping process of ceramics will have a key role in the quality of the final piece. Indeed, the chosen process will directly impact the microstructure of the material. Generally speaking, ceramics are produced from densified powders using high-temperature processes. An external element will generate heat which will then be diffused into the material. One of the main issues with these processes is that, unlike polymers and metals, ceramics have very high processing temperatures due to their high melting point. This will therefore lead to high energy consumption and thus higher production costs. In response to this problem, new processes are being developed to manufacture ceramics using less energy. These new technologies also make it possible to obtain similar or even better properties than those obtained by conventional methods. (Alvaro, 2016)

This project investigates an alternative process, that is microwave sintering. This process is based on the action of an electromagnetic wave, which seems to be interesting since nickel-zinc ferrite has good electrical and magnetic properties. This process has many advantages such as shorter processing times leading to lower energy consumption, higher heating rates and an uniformity in the heating process. As densification mechanisms are different during microwave sintering, it is possible to obtain finer microstructure with an important densification. (Alvaro, 2016) Finally, this process of sintering seems to be cleaner and more environment friendly than conventional processes.

Objectives

The first aim of this project is therefore to study the sinterability of a composite of 16 vol% nickel-zinc ferrite and 84 vol% alumina. Two different sintering processes will be used: conventional sintering and microwave sintering as well as different time and temperature parameters.

The second objective is to study the mechanical properties and microstructure of this composite.

1) State of the art – Materials studied

This section is intended to review the different materials investigated in this report. The following sub-sections will deal with their mechanical and physical properties such as their crystalline structure as well as their electrical behaviour.

1.1. Nickel-Zinc Ferrites

Nickel-Zinc ferrites are known to have a high electrical resistivity and good magnetic properties. This combined with their low cost and high formability makes it the material of choice for antenna rods, loading coils, read/write heads for high-speed digital tape, power transformers in electronics, telecommunication application and microwave devices. (Yadoji, Peelamedu, Agrawal, & Roy, 2003)

This kind of ferrites are often prepared by conventional sintering, which makes it difficult to control the final microstructure and stoichiometry of the components. During conventional sintering, the samples are heated at high temperatures for long periods of time, which can cause the evaporation of certain constituents and thus change the stoichiometry. (Costaa, Tortellab, Morelli, & Kiminami, 2003) Since Ni-Zn ferrites absorb microwaves very well, manufacturing them by microwave sintering seems to be an interesting alternative to overcome this kind of problem.

1.1.1 Crystallographic structure

Ferrites are ionic compounds consisting mainly of trivalent iron and oxygen. The general formula of nickel-zinc ferrite is $Ni_xZn_yFe_2O_4$ with the sum of x and y equal to 1. This is a spinel ferrite with an AB_2O_4 structure where A represents the tetrahedral sites and B the octahedral sites. As illustrated in Figure 1-1, zinc atoms have a preference for tetrahedral sites while nickel atoms prefer octahedral ones. Iron atoms, on the other hand, are distributed over both sites. (Ali, Khan, Chowdhury, Akhter, & Uddin)

O^{2-}

Tetrahedral   Octahedral
sites Zn^{2+} sites Ni^{2+}
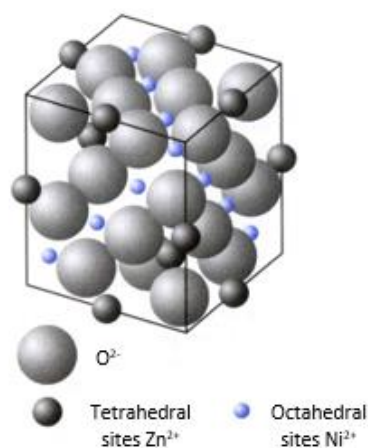
FIGURE 1-1. STRUCTURE OF NICKEL-ZINC FERRITE (LAPOINTE, 2010).

The crystallographic properties of Ni-Zn ferrites (Table 1.1) were determined in Gaëlla Frajer's thesis. (Frajer, 2018) To calculate the theoretical density, the author used the following formula:

$$\rho_{theoritical} \; = \frac{8M}{Na \cdot a^3} \; [g \cdot cm^{-3}]$$

(1.1)

With M the molar mass (g·mol^{-1}), Na the Avogadro number equal to 6,022·10^{23} mol^{-1} and a the lattice parameter (cm).

Ferrite	a (Å)	M (g·mol^{-1})	ρ (g·cm^{-3})
$Ni_{0,5}Zn_{0,5}Fe_2O_4$	8,40	238	5,34

TABLE 1-1. CRYSTALLOGRAPHIC PROPERTIES OF NI-ZN FERRITES.

1.1.2 Properties

- *Magnetic structure and saturation polarisation*

The octahedral and tetrahedral sites will form two sub-networks that will interact indirectly through oxygen ions. This phenomenon is called "super-exchange" and there are three different types: A-A, B-B and A-B. In Ni-Zn ferrites the A-B exchanges are predominant. Hence, it leads to the formation of two sites of opposite signs whose moments do not automatically compensate each other. This phenomenon will lead to a spontaneous magnetisation of the material, which is characteristic of ferrimagnetic materials. (Frajer, 2018)

It is known that the total resulting magnetisation is equal to the difference between the magnetisation of lattice A and the magnetisation of lattice B. The Zn^{2+} ions, which have no magnetic moment, play an important role. In fact, they will initially increase the difference in magnetisation between the two sub-networks, giving the Ni-Zn ferrite greater magnetising properties than other ones. However, if the quantity of zinc is too high, the interactions between the sub-networks will be too low to keep the magnetic moments parallel. Table 1.2 illustrates this phenomenon. (Lebourgeois, 2005)

Ferrite	Magnetic structure at 25 °C	Saturation polarisation Js at 25 °C
$Ni_{0,2}Zn_{0,8}Fe_2O_4$	paramagnetic	≈ 0
$Ni_{0,5}Zn_{0,5}Fe_2O_4$	ferrimagnetic	0,53
$NiFe_2O_4$	ferrimagnetic	0,33

TABLE 1-2. INFLUENCE OF ZINC CONTENT ON MAGNETIC STRUCTURE AND MAGNETIC SATURATION POLARISATION OF NI-ZN FERRITES. (LEBOURGEOIS, 2005)

The magnetisation is maximum at a temperature of 0 K and drops with the increase of temperature.

Another property of nickel-zinc ferrites is its low magnetic coercivity.

The coercivity of a material is characterised by its ability to withstand an external magnetic field without becoming demagnetised. Ni-Zn ferrites therefore belong to the category of soft ferrimagnetic materials. (Yadoji, Peelamedu, Agrawal, & Roy, 2003)

- *Curie temperature Tc*

The Curie temperature is the temperature at which a ferrimagnetic material becomes paramagnetic, which means that it loses its spontaneous magnetisation. This temperature varies according to various parameters such as the composition of the ferrite or the exchange interaction value of the A and B networks. Indeed, as seen previously, the interactions decrease with the increasement of zinc level.

The Curie temperature will therefore decrease when the zinc rate increases. In the case of nickel-zinc ferrite, the Curie temperature varies from 585 °C for a nickel ferrite to around 100 °C for a $Ni_{0.3}Zn_{0.7}Fe_2O_4$ ferrite. (Lebourgeois, 2005)

- *Magnetostriction*

Magnetostriction is characterised by the ability of a magnetic material to be deformed under the effect of a magnetic field or, on the contrary, to create a magnetic moment under the effect of mechanical stress.

The strain is maximal when the magnetization is at saturation. In this case, the saturation magnetostriction coefficient is maximal and noted λs. If this coefficient is negative, a contraction is observed. On the contrary, if the coefficient is positive, an elongation is observed. In the case of nickel-zinc ferrite, the coefficient varies from $-26 \cdot 10^{-6}$ for a nickel ferrite to $-1 \cdot 10^{-6}$ for a zinc-rich ferrite. (Lebourgeois, 2005)

- *Electrical resistivity*

The electrical resistivity of a material is its ability to oppose the flow of electric current. As a reminder, ferrites are composed of oxygen ions and metal cations. The resistivity will therefore depend on the nature of the cations, their valency but also on the defects present, whether they are cationic or anionic vacancies or ions in interstitial positions. (8)

Ni-Zn ferrites have a very high electrical resistivity, $\rho > 10^5$ Ω·cm (Lebourgeois, 2005), which makes them very useful in high frequency applications. As a matter of fact, such high electrical resistivity implies that the eddy current losses are very low and sometimes they can be neglected. These losses characterise the power dissipated by the Joule effect linked to the flow of current induced in the material. (7)

- *Mechanical and chemical properties*

Ferrites have very poor mechanical properties. Indeed, their tensile fracture stress varies between 20 and $70 \cdot 10^6$ Pa, their compressive fracture stress between $0,2 \cdot 10^9$ and $0,7 \cdot 10^9$ Pa and their Young's modulus between $80 \cdot 10^9$ and $150 \cdot 10^9$ Pa.

These properties will also depend on the density of the material. Indeed, for an additional porosity of 10%, the properties will be decreased by two times. (Lebourgeois, 2005)

Despite their low mechanical properties, ferrites are characterised by high hardness and therefore good abrasion resistance. They are also thermally insulating, with a thermal conductivity closer to resins than to metals (Table 1.3).

Material	Ferrite	Resin	Copper
Thermal conductivity ($W \cdot m^{-1} \cdot K^{-1}$)	4 to 5	2 to 3	400

TABLE 1-3. THERMAL CONDUCTIVITY OF FERRITES, RESINS AND COPPER.

Finally, from a chemical point of view, ferrites are inert and unaffected by humidity and other atmospheric conditions. They are soluble only in a hot and acidic environment, which gives them a great range of use. (Lebourgeois, 2005)

1.2 Alumina

Nowadays alumina is a material of great importance. Although its main use is to produce aluminium, it is also found in many different fields. (Croquesel, 2015) Alumina with high densities (around 99.8%) is often used in very high temperature applications as refractory material. Alumina with lower densities (around 80-90%) is used for lower temperature applications as electrical insulators or mechanical components. Finally, due to its high hardness, alumina is also present in cutting materials, bearings, pump components… (Borrell Tomás & Salvador Moya, 2018)

1.2.1 Manufacturing and crystallographic structure

Alumina, of formula Al_2O_3, is an aluminium oxide generally synthesised from Bauxite, an aluminium hydroxide by mean of the Bayer process. Bauxite consists of various hydrated aluminium oxides as well as iron oxides, quartz and clay. During this process, the alumina in the bauxite is dissolved in caustic soda at high temperature and pressure to precipitate the alumina hydrate. (Croquesel, 2015) There are several precursors in Bauxite that can be used to obtain alumina: Gibbsite or Hydrargillite (γ-Al(OH)$_3$), Bayerite (α-Al(OH)$_3$), Nordstrandite (β-Al(OH)$_3$), Boehmite (γ-(Al(OOH)) and Diaspore (α-Al(OOH)). (Levin & Brandon, 1998) The alumina hydrate is then calcined to obtain alumina. One of the disadvantages of this process is that it does not produce ultra-pure alumina. To obtain a higher purity of alumina (>99.98%), the alum process has to be used. This process consists of dissolving aluminium hydrate produced by the Bayer process in sulphuric acid in the presence of ammonium. The product, called ammonium alum, is then crystallised by cooling and calcined. (Mauss, 1994)

As illustrated in Figure 1.2 (Levin & Brandon, 1998), depending on the starting aluminium hydroxide, different transition alumina (γ, δ, θ, χ, κ, η) with different crystallographic structures are obtained.
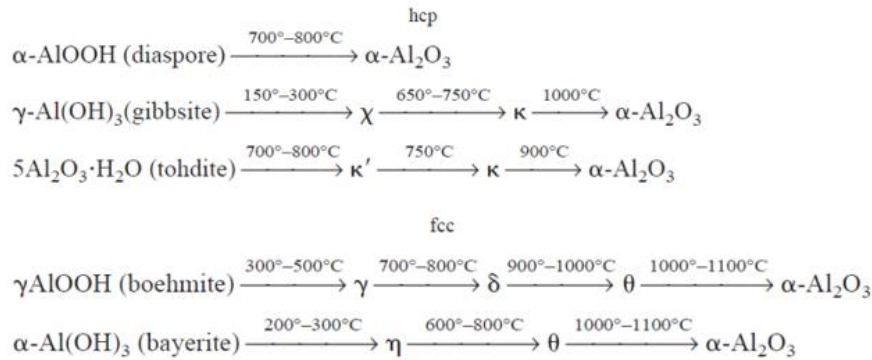
FIGURE 1-2. TRANSFORMATION SEQUENCES FROM METASTABLE ALUMINA TO STABLE ALUMINA FORMATION.

There is only one thermodynamically stable phase of aluminium oxide, α-alumina, which is obtained at temperatures above 1100-1200 °C. This alumina, commonly known as corundum, crystallises in the orthorhombic system. This structure is characterised by a hexagonal mesh with the following parameters (Croquesel, 2015):

$$a = 4{,}759 \,\text{Å} \qquad c = 12{,}991 \,\text{Å} \qquad \alpha = \beta = 90° \qquad \gamma = 120°$$

Oxygen ions form a hexagonal stack along the c-axis. Each aluminium ion is bound to 6 oxygen and occupies an octahedral interstice between the layers formed by the oxygen ions. To maintain the electrical equilibrium, only 2/3 of the octahedral interstitial sites are occupied by Al^{3+} ions. (Borrell Tomás & Salvador Moya, 2018)

Figure 1.3 (Borrell Tomás & Salvador Moya, 2018) illustrates the compact hexagonal structure of α-Al_2O_3. O^{2-} ions are located in layers A and B while Al^{3+} ions are in layers a, b and c.
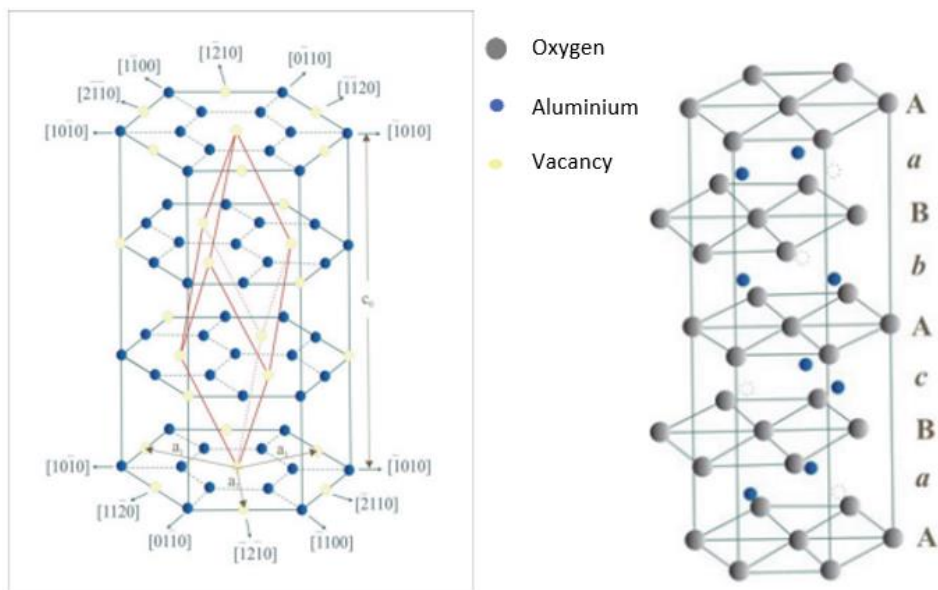
FIGURE 1-3. HEXAGONAL STRUCTURE OF ALPHA-Al_2O_3 AND STACKING SEQUENCE AABBACBAA.

1.2.2. Properties

The alpha phase of alumina is the most widely used phase because of its very good properties and it is the only phase that is thermodynamically stable over a wide range of temperatures. α-Al_2O_3 is known for its resistance to abrasion, its high mechanical and chemical resistance, and its electrical resistance. Indeed, α-alumina is a very good electrical insulator. Table 1.4 shows the main properties of α-Al_2O_3.

Property	Value
Colour	Translucent white
Melting temperature (°C)	2100
Density (g/cm^3)	3,985
Young's modulus (GPa)	380
Stiffness modulus (GPa)	162
Vickers hardness (GPa)	15-20
Tensile strength (MPa)	260-300
Bending strength (MPa)	280-900
Compressive strength (MPa)	2200-2600
Toughness Kic (MPa.m$^{1/2}$)	2,7-4,2
Thermal conductivity (W.m^{-1}. K^{-1})	30-40 at 100°C

TABLE 1-4. PHYSICAL AND MECHANICAL PROPERTIES OF 99.9% PURE ALPHA-ALUMINA.

Thus, as shown previously, alumina has very good mechanical properties but is a dielectric material that have few interactions with microwaves. On the contrary, Ni-Zn ferrite has poor mechanical properties but good mechanical properties and high electrical resistivity. The interest of manufacturing a composite made of 16 vol% ferrite and 84 vol% of alumina is therefore to combine both properties of these two materials.

2) State of the art: Sintering

During the sintering process, a ceramic powder is heated at very high temperatures in order to achieve complete densification of the material. This process is carried out at temperatures below the melting or degradation temperature of the material. Thanks to this thermal energy, bonds between the grains of the material will be created and will grow by atomic or molecular diffusion. The aim is to obtain a more compact solid, with less porosity and therefore better properties.

This process can be carried out in two different ways: in the solid state or in the liquid phase. In liquid phase sintering process, the solid grain coexists with a wetting liquid, whereas in solid state sintering only the solid phase is involved. During this project, only solid phase sintering is studied.

2.1. Generality

2.1.1 Principle of sintering

The driving force of sintering is the lowering of the free energy of the system by two ways: densification and growth and coalescence of the grains. In a system without liquid phase, the free enthalpy variation is equal to:

$$\Delta G = \gamma_{SG} * \Delta A_{SG} + \gamma_{SS} * \Delta A_{SS} + p * \Delta V \qquad (2.1)$$

with γ_{SG} and γ_{SS} respectively the surface energies of the solid-gas (pores) and solid-solid (grain boundaries) interfaces, ΔA_{SG} and ΔA_{SS} the variations in the areas of the solid-gas and solid-solid interfaces, p the applied pressure and V the volume of the sample. (Croquesel, 2015)

Depending on the nature of the phases in contact, solid-gas or solid-solid, the surface energy will change. As shown in Table 2.1 (Bernache-Assolant & Bonnet, 2005), the surface energy is higher for solid-gas interfaces than for solid-solid interfaces.

Type of interface	Surface energy ($J \cdot m^{-2}$)
Solid-gas	0,1 to 1
Solid-solid	0,01 to 1

TABLE 2-1. SURFACE ENERGIES OF DIFFERENT INTERFACES.

The material will therefore try to reduce these solid-gas interfaces and form less energetic solid-solid interfaces. (Alvaro, 2016) The particles will therefore change shape and their centres will move closer together. The initial surface of the particles will therefore gradually become the grain boundary during the process.

One of the key factors for densification to occur is that the energy of the grain boundary γ_{BG} must be half of the surface energy of the solid-gas interface γ_{SG}. This implies that the angle formed by two grains, called the dihedral equilibrium angle, must measure less than 180° (Figure 2.1). This angle is related to the energy at the grain boundary by the equation (Borrell Tomás & Salvador Moya, 2018):

$$\gamma_{BG} = 2 \cdot \gamma_{SG} \cdot \cos\left(\frac{\varphi}{2}\right) \qquad (2.2)$$
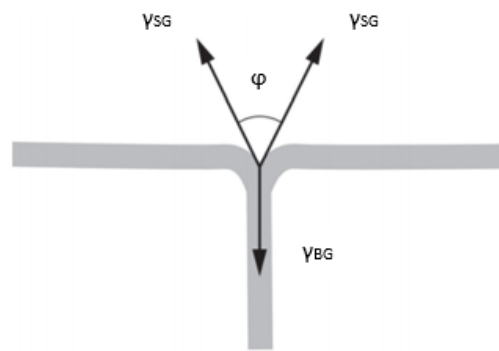
FIGURE 2-1. DIHEDRAL EQUILIBRIUM ANGLE FORMED BY TWO GRAINS.

2.1.2 Mechanisms of mass transport

Solid phase sintering is a complex mechanism involving 6 different mass transport mechanisms represented in Figure 2.2. (Alvaro, 2016)

1- Surface diffusion: The material moves along the surface of the particles up to the neck region. This mechanism takes place at the beginning of the process.
2- Lattice diffusion (vacancies): Vacancies move around in the lattice creating a transfer of material to the neck.
3- Vapor transport: The material near the neck area evaporates before condensing in the neck.
4- Boundary diffusion: The mass transfer is due to an important disorientation of atoms at grain boundaries.
5- Lattice diffusion (grain boundaries): The material moves along the grain boundary from the inside of the particle to the surface.
6- Lattice diffusion (dislocations): The dislocations will be used as vacancies which will create a transfer of material to the neck region.
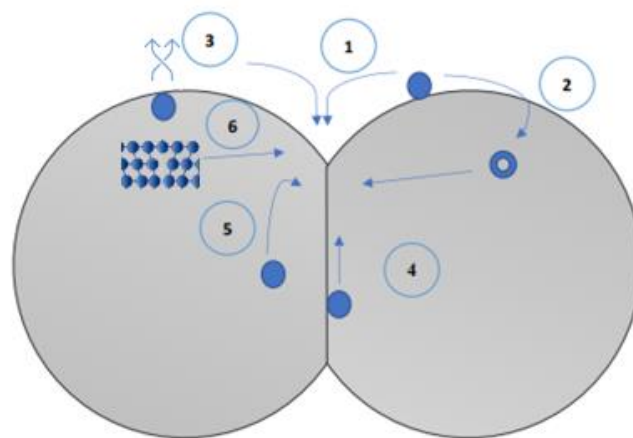
FIGURE 2-2. MASS TRANSPORT MECHANISMS. (RAHAMAN, 2007)

19

Although all these mechanisms contribute to the formation of necks between particles, they do not all allow the densification of the material. Indeed, the mechanisms where the source of the material comes from the surface or the neck area, do not allow the centres of the particles to move closer together and thus densify the material. However, they do allow a modification of the shape of the pores and increase the strength of the material. (Borrell Tomás & Salvador Moya, 2018) These mechanisms are therefore the surface diffusion, the vapor transport, and the lattice diffusion from the surface to the neck. The boundary diffusion and the lattice diffusion by grain boundaries mechanisms are those which play an essential role in the densification of the material.

2.1.3 The sintering steps

As shown in Figure 2.3, sintering process consists of three different steps. A preliminary step of powder forming (usually by compaction) has already been carried out in order to create contacts between the particles. (Alvaro, 2016)
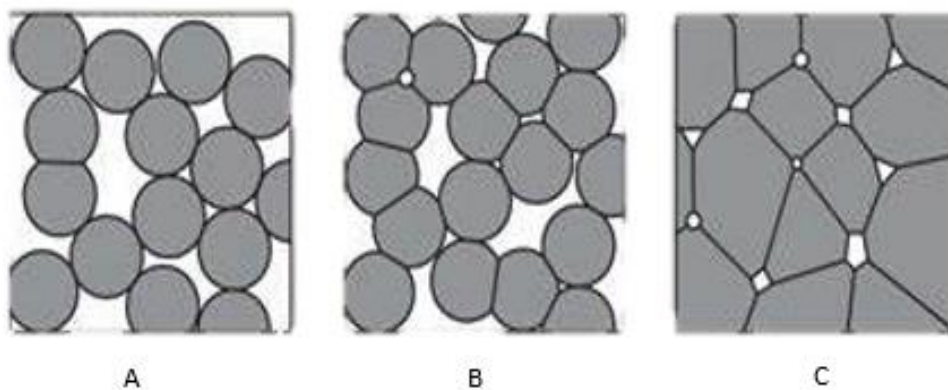
FIGURE 2-3. SINTERING STEPS: A) INITIAL STAGE, B) INTERMEDIATE STAGE, AND C) FINAL STAGE.

The first stage of sintering is characterised by the formation and growth of necks between the particles, thus reducing the free energy of the system as explained above. The diffusion mechanisms are activated by a gradient in the chemical potential between the necks formed by two particles and the surface of those particles. This gradient will allow the material to converge towards the neck area which will lead to the growth of the necks and a phenomenon of shrinkage of the particles. The initial stage ends when the ration between the radius of the neck and the radius of the particle is equal to 0,4. At this moment, the relative density is around 65%. (Alvaro, 2016)

The second stage, known as the intermediate stage, is the step where most of the microstructure changes and densification take place. The size of the porosities will gradually drop, and the grains become interconnected. The end of this stage is characterised by the emergence of isolated pores and the relative density of the material is around 92%. (Croquesel, 2015)

The final stage of sintering is a decisive step for the properties of the material. The aim of this step is to remove the remaining pores in order to achieve a relative density of more than 95%. At this stage of the process, granular growth will compete with densification and therefore time and temperature become very important factors. (Alvaro, 2016) Increasing them will indeed allow the elimination of pores but can also cause excessive growth of the grains. The latter can nonetheless be inhibited by the addition of dopant in the raw powder.

2.1.4 Influent parameters of sintering processes

There are many parameters influencing sintering. These parameters can be separated into two categories: process related parameters and material related parameters. These parameters are listed in Table 2.2. (Borrell Tomás & Salvador Moya, 2018)

Material related parameters	Process related parameters
Particle shape	Temperature
Particle size	Time
Size distribution	Pressure
Particle dispersion	Atmosphere
Composition	Heating/Cooling rate
Purity grade	Heat source
Homogeneity	

TABLE 2-2. VARIABLES THAT AFFECT SINTERING AND MICROSTRUCTURE. (BORRELL TOMÁS & SALVADOR MOYA, 2018)

2.2 Conventional Sintering

Conventional sintering is a very old sintering technique used for both technical and traditional ceramics. During this process, a compacted powder is heated in a conventional oven at very high temperatures (between 1000 and 1800 °C) for several hours. (Alvaro, 2016) The oven has resistances which, by Joule effect, will heat and radiate on the material. In order to calibrate ovens, sintering rings are used. By measuring their diameter, the exact firing temperature can be determined.

Parts will be heated from the surface to the bulk of the material using three heat transfer mechanisms: conduction, radiation, and convection. To obtain a temperature homogenization and a uniform heat distribution, a long heating time will be necessary. This long process time, resulting in high energy consumption, are the major disadvantages of conventional sintering.

In order to overcome these disadvantages, new non-conventional sintering processes have been developed and one of these promising techniques is microwave sintering.

2.3 Microwave Sintering

The use of microwaves as a heat source has been known for a long time, especially for water and food products. In recent years, microwave sintering has attracted a lot of interest due to its many advantages compared to conventional sintering methods. Many researchers have shown that this method allows powders to be consolidated quickly at lower temperatures while maintaining a grain size similar to the original powder. This technique therefore makes it possible to obtain better properties more rapidly and with less energy consumption. (Oghbaei & Mirzaee, 2010) (Sutton, 1992)

In recent years, research on microwave sintering has begun to focus on the manufacture of ceramic composites with the aim of improving their structural and functional properties so that they can be used in several industrial fields. (Borrell Tomás & Salvador Moya, 2018)

2.3.1 Microwave heating fundamentals

- *Microwaves in the electromagnetic spectrum*

Microwaves correspond to the less energetic zone of the microwave spectrum. (Borrell Tomás & Salvador Moya, 2018) Indeed, they have a wavelength λ between 1 m and 1 mm, i.e. a frequency between 300 MHz and 300 GHz (Figure 2.4). These waves are mainly used in applications such as telecommunications and heating. Domestic microwave ovens have a frequency around 2.45 GHz. (Alvaro, 2016) Some microwave ovens, especially those used to study the influence of frequency on the dielectric properties of materials, can go to frequencies between 915 MHz (Katz, 1992) and 83 GHz (Sano & Makino, 2000). It is important to note that the use of high frequencies allows a more uniform distribution of the electric field to be obtained but also represents a much higher cost.
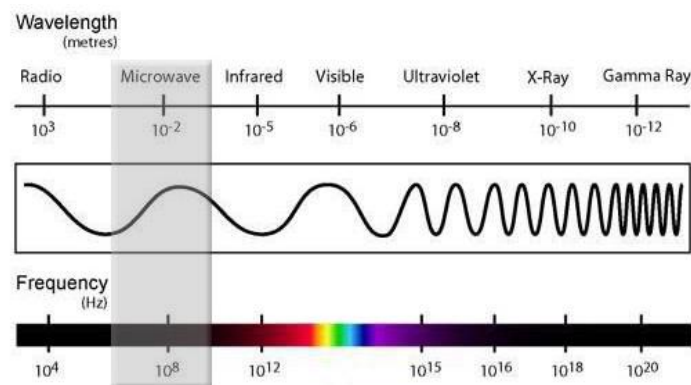
FIGURE 2-4. ELECTROMAGNETIC SPECTRUM.

Like all electromagnetic waves, microwaves are characterised by the free and guided propagation of an electromagnetic field $\vec{E}$ (V/m) and a transverse magnetic field $\vec{H}$ (A/m). As shown in Figure 2.5, these two fields define a plane perpendicular to the propagation vector $\vec{k}$ with $\vec{k} = \frac{2 \cdot \pi}{\lambda}$. (Croquesel, 2015)
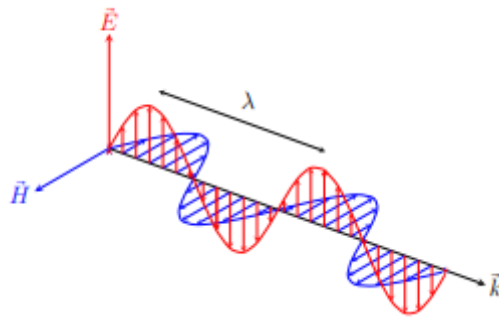
FIGURE 2-5. ELECTROMAGNETIC WAVE.

- *Interaction of Microwaves with Matter: macroscopic scale*

Depending on its electrical and magnetic properties, a material can interact with microwaves in different ways. The depth of penetration of the electric or magnetic field is inversely proportional to its electrical conductivity. As shown in Figure 2.6, it can be:

- Transparent: Microwaves enter and exit the material without any energy transfer. This is the case with low loss insulating materials such as alumina (T<1000 °C), magnesium oxide or silica.
-Opaque: Microwaves are reflected at the surface of the material, so there is no energy transfer. These materials are called conductors (this is generally the case with metals).
-Absorbent: Microwaves are absorbed by their material and there is an exchange of electromagnetic energy. The amount absorbed varies according to the dielectric properties of the material.
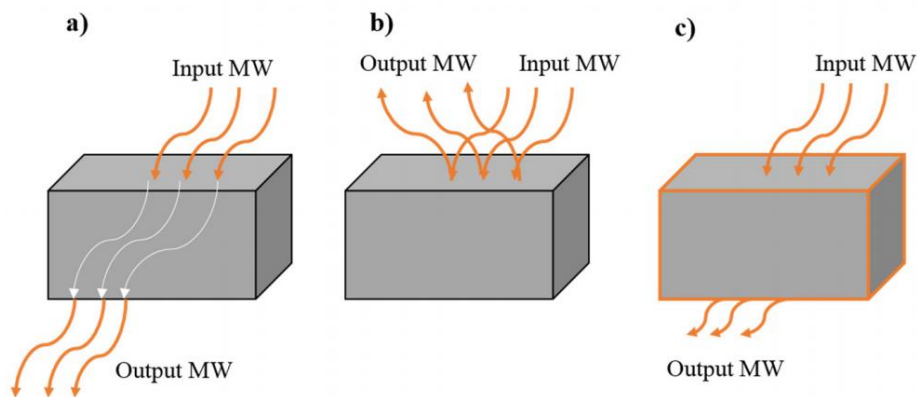
FIGURE 2-6. MATERIAL/MICROWAVE INTERACTION: A) TRANSPARENT, B) OPAQUE, AND C) ABSORBENT.

A material must therefore be absorbent to be heated by microwaves. However, it is important to note that above a certain so-called critical temperature, some materials (such as zirconia at 500°C) can become absorbent and heat up quickly. On the contrary, at high temperatures, some materials will become more and more electrically conductive and thus reflect the field. The coupling of the field with microwaves will then decrease and may stop the heating.

In addition, microwave heating can also be carried out on opaque or transparent materials using a material called susceptor. This indirect heating technique is based on the use of a material that exchanges with microwaves at low temperatures and allows the sample to be heated by conduction and/or radiation (Figure 2.7-a). If the properties of the material increase as its temperature rises and can interact with microwaves from a certain temperature, it is called hybrid heating. (Borrell Tomás & Salvador Moya, 2018) Indeed, the sample is heated by the susceptor and the microwaves (Figure 2.7-b) This principle is illustrated in Figure 1.10.
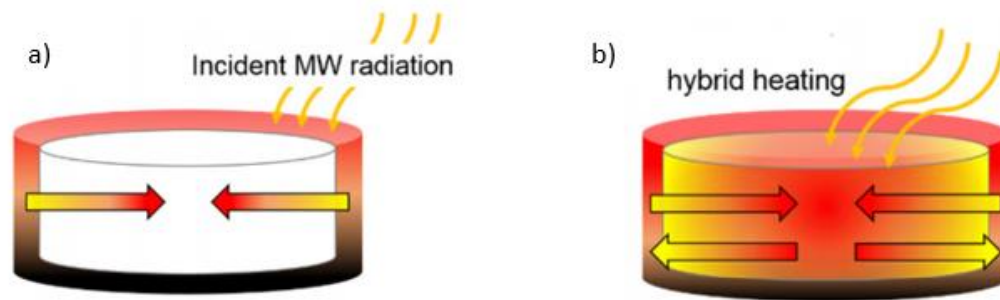
FIGURE 2-7. PRINCIPLE OF HYBRID HEATING: A) THE SAMPLE IS HEATED BY THE SUSCEPTOR B) THE SAMPLE IS HEATED BY THE SUSCEPTOR AND THE MICROWAVES.

During this project, a silicon carbide susceptor will be used with the composite.

- Heating mechanisms

Heating mechanisms can be divided into two categories: those related to the electric fields and those related to the magnetic fields.

Non-magnetic materials are in fact only impacted by the electrical part of the electromagnetic wave. The penetration of an electromagnetic field into a dielectric material leads to the creation of an internal electric field in the material. This will cause dipole rotation movements and the translation of bound charges such as valence electrons and ions, but also conduction electrons in the case of non-perfect dielectrics. The inertial, frictional, and elastic forces will then be at the origin of a phenomenon of resistance to these induced movements which will cause losses and attenuation of the electric field. In a non-perfect dielectric material subjected to an alternating electric field, there are two phenomena which cause losses:

- the dielectric polarisation caused by the simultaneous displacement of positive and negative bonded charges.
  the electrical conduction caused by the displacement of free charges of the same sign.

These dielectric losses will thus by Joule effect allow the material to be heated by volume. (Guyon, 2013) Dipole losses are mostly present in electrical insulating materials, whereas conduction losses are mostly present in metallic and high conductivity materials.

It is accepted that magnetic losses are close to zero in the microwave range for most ceramic oxides. However, magnetic materials such as ferrites are affected by the electric but also the magnetic field too. When a conductive material is subjected to an alternating magnetic field, an electromotive force is generated. This electromotive force will induce electric currents called eddy currents. These currents are a consequence of the magnetic induction of the material and have two consequences: the creation of a magnetic field opposing the cause that gave rise to it (Lenz's law) and the appearance of heating by Joule effect. (Guyon, 2013)

2.3.2 Microwave installation

The purpose of this part is to describe the different components of a microwave used for sintering. A microwave is composed of several parts including 3 main components: a microwave generator that will generate the electromagnetic radiation, a transmission line allowing the circulation of microwaves and a resonant cavity in which waves and matter interact. Figure 2.8 shows a rectangular cavity microwave system from ITACA-UPV (Instituto de Aplicaciones de las Tecnologías de la Información y de las Comunicaciones Avanzadas de la Universidad Politécnica de Valencia. (Borrell, Dolores Salvador, . Penaranda-Foix, & Catala-Civera, 2013; Benavente, et al., 2014)
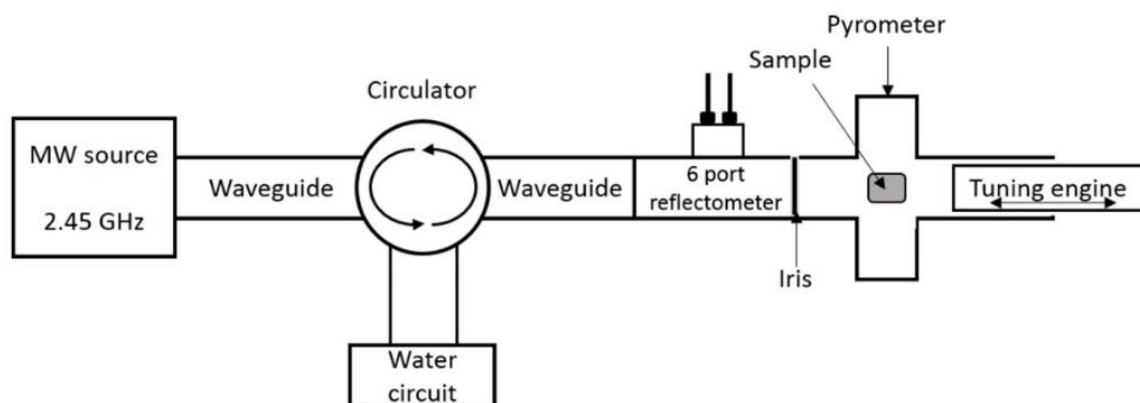
FIGURE 2-8. SCHEMATIC OF A MICROWAVE WITH A RECTANGULAR CAVITY. (ALVARO, 2016)

-   Microwave generator

There are several types of microwave generators such as klystrons, gyrotrons and magnetrons. In our case the generator used is a magnetron, generating a frequency of 2.45 GHz. The role of the generator is to transform low-frequency electrical energy into high-frequency electromagnetic energy. (Guyon, 2013)

A magnetron consists in a metal cylinder serving as an anode, in which are dug reasoning cavities that communicate with a central cavity (Figure 2.9). In the middle of this cylinder is a filament acting as cathode.
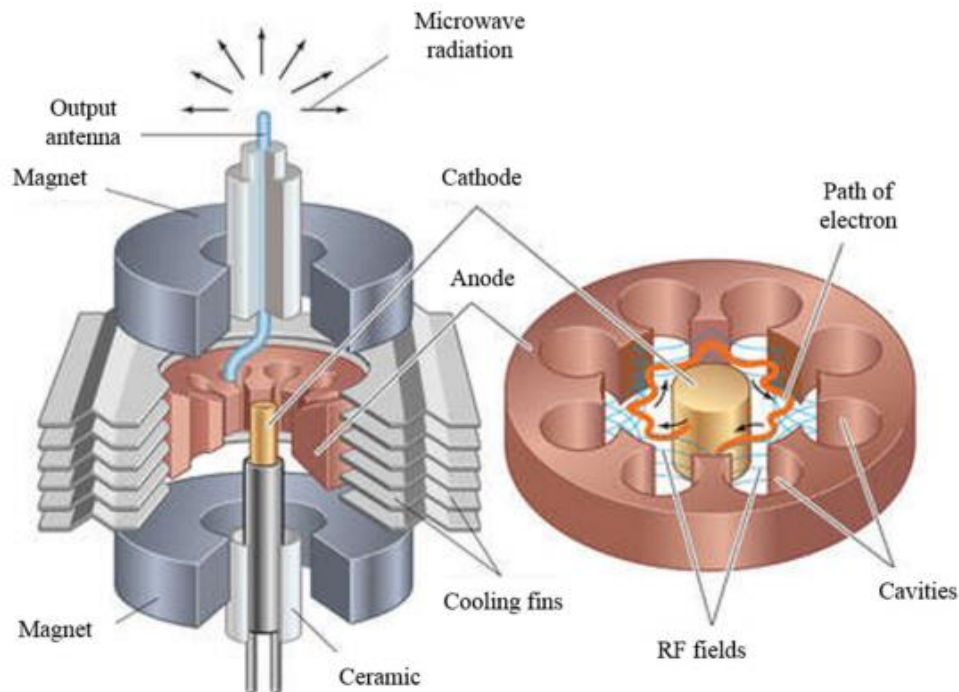
FIGURE 2-9. REPRESENTATION OF A MAGNETRON. (ALVARO, 2016)

By applying a potential difference of several kV between the cathode and the anode, a radial and continuous electric field is created. The filament, traversed by a flow of current, heats up and emits electrons which are then accelerated and attracted by the cathode. At both ends of the cylinder are permanent magnets that generate an axial magnetic field perpendicular to the electric field. This will consequently change the trajectory of the electrons into a helical trajectory. (Croquesel, 2015)

The electrons will polarize the anode and induce currents around the reasoning cavities. These currents are then at the origin of a magnetic field oscillating at a given frequency. This frequency will vary according to the geometry and the number of cavities. (Croquesel, 2015) The electrons are either slowed down or accelerated by the cavities, creating an oscillation of charges. An antenna will finally create microwaves from this charge oscillation.

- Waveguide

Waveguides lead the microwave radiation from the generator to the main cavity where our sample is located. It is necessary to use circular or rectangular waveguides. Indeed, the use of simple coaxial cables is not conceivable for this type of high frequency application because the losses would be too high. (Alvaro, 2016) In our case, a rectangular waveguide will be used.

The propagation of an electromagnetic wave can take place in two different ways in a waveguide: according to the TE (Transverse Electric) mode or according to the TM (Transverse Magnetic) mode. In the TE mode, the component of the electric field in the direction of propagation is null whereas in the TM mode, it is the magnetic component. (Guyon, 2013)

- Circulator

The circulator protects the microwave source from possible waves that may not be consumed and reflected by the material. These waves are thus redirected towards a load of water which will then heat up. (Borrell Tomás & Salvador Moya, 2018)

- 6 ports reflectometer

The 6 ports reflectometer allows the incident and reflected power to be measured in order to obtain the real power used when sintering the material. (Borrell Tomás & Salvador Moya, 2018)

- Iris

The iris is used for coupling the microwave power to the cavity. (Borrell Tomás & Salvador Moya, 2018)

- Pyrometer

The pyrometer enables the temperature of the sample to be measured precisely and continuously. In conventional sintering the temperature is measured directly with a thermocouple located in the oven. This is not possible during microwave sintering because the device could interfere with the process. In addition, one of the characteristics of microwave heating is that the radiation is absorbed by the material, allowing the sample to be heated volumetrically. The temperature of the sample and the temperature of the oven are therefore often different. (Alvaro, 2016)

A pyrometer consists of an optical system and a detector based on Stefan Boltzmann's law:

$$j^* = \varepsilon \cdot \sigma \cdot T^4 \qquad (2.3)$$

With j* the thermal radiation, ε the emissivity, T the temperature and σ Stefan Boltzmann's constant equal to 5.670 W·m^{-2}·K^{-4}.

This system therefore makes it possible to relate the heat radiation j* to the temperature of the sample T without coming into contact with it. For this, however, it is necessary to know the emissivity of the material. The determination of the emissivity of Ni-Zn ferrite will be developed in part 3.2.

- Resonant cavity

The resonant cavity is the key part of the microwave. This is where the material is heated and sintered by the electromagnetic wave. There are several types of resonant cavity: monomodal, multimodal or multimodal with variable frequency.

In this study a rectangular single-mode cavity is used. The size of a monomodal cavity is of the order of one wavelength and allows the sintering of small parts ranging from 1 to 5 cm. (Croquesel, 2015) This type of cavity is therefore of great interest in the research community but has limited use in the industrial environment.

A single-mode cavity can be described as a dielectric volume surrounded by conductive surfaces. This type of cavity is limited to a single mode of propagation of the electromagnetic wave. As previously explained with waveguides, one mode represents a TE or TM type configuration. In a single-wave cavity, a standing wave is formed with the minima and maxima of the known $\vec{E}$ and $\vec{H}$ fields. (Guyon, 2013) During this study, the samples will be sintered using the magnetic part of the electromagnetic wave.

- Tuning engine

This element makes it possible to control the dimensions of the cavity in order to optimise the energy consumption of the microwaves.

3) Materials and methods

As stated previously, the aim of this project is to compare two different sintering methods: conventional sintering and non-conventional microwave sintering. The second objective of this project is to study the properties of a composite consisting of 16 vol% alumina and 84 vol% Ni-Zn ferrite. The sintering time and temperature will be varied in order to study their influence on the material properties.

3.1 Materials

The alumina powder used is a commercial α-alumina powder prepared by Taimei Chemicals (Japan). This alumina has a very high purity (>99%) and a density equal to 3,985 g/cm^3. The main properties of α-alumina are explained in the part 1.2.2.

The Ni-Zn ferrite powder used is a commercial powder manufactured by Ferroxcube. The formula of this ferrite is $Ni_{0,5}Zn_{0,5}Fe_2O_4$. Table 3.1 shows the different properties of the $Ni_{0,5}Zn_{0,5}Fe_2O_4$ from Ferroxcube.

Properties	Value
Density	5,70 $g.cm^{-3}$
Average grain size	1,7 μm
Electrical resistivity	10^5 Ω.cm
Curie temperature	125°C

TABLE 3-1. PROPERTIES OF NI-ZN FERRITE FROM FERROXCUBE.

The composite is made of 16 vol% Ni-Zn ferrite and 84 vol% alumina.

3.2 Methods

3.2.1 Compaction

The forming of powders by compacting makes it possible to obtain a part with specific dimensions and geometry. In this study, the powders were compacted by cold isostatic pressing (CIP). The compression fluid used is water. 1 g of powder is placed in a deformable rubber balloon in order to isolate it from the compression fluid. The balloon is tightened and closed to form a ball of powder and immersed in the fluid. The pressure is applied in a pressure vessel via a liquid. This pressure is then transmitted to the part equally in all direction. (Lorraine F, 2016)

The isostatic compaction of the powders results in a round piece with a homogeneous density. The isostatic press used is shown in Figure 3.1.

FIGURE 3-1. COLD ISOSTATIC PRESSING (CIP).

3.2.2 Sintering

Conventional sintering is carried out in a furnace Carbolite Gero HTF 1800 (Figure 3.2) at temperatures ranging from 1000 to 1400 °C for 1 or 2 hours. The heating rate during the process is 10°C/min.

FIGURE 3-2. FURNACE USED FOR CONVENTIONAL SINTERING.

Microwave sintering was carried out in a monomodal rectangular cavity using the magnetic part of the electromagnetic wave. The power of the microwave used is 800 W and the frequency is 2.45 GHz.

In order to be able to calibrate the pyrometer, the emissivity of the 16 vol% (Ni-Zn) ferrite-alumina composite was determined. For this purpose, a sample is heated in a conventional oven. The temperature is measured using both the thermocouple in the oven and the pyrometer placed above the oven. The pyrometer used is from the commercial firm OPTRIS, model G5H (CF2) and the temperature ranges are from 250 to 1650 ºC. The oven is programmed to heat and stabilize at given temperatures (1000, 1100 and 1200 °C). Figure 3.3 shows the scheme of the measurement area according to the manufacturer:
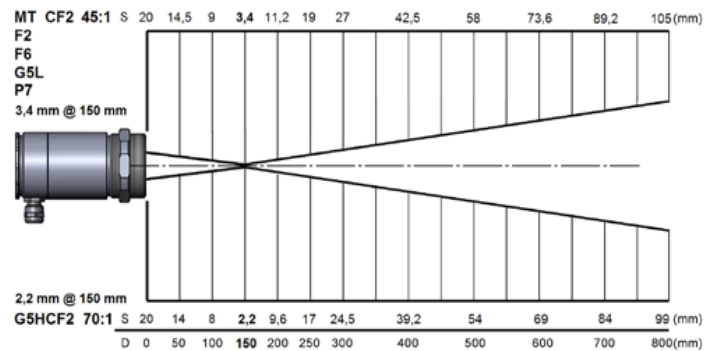
FIGURE 3-3. DIMENSIONS OF THE MEASUREMENT AREA OF THE G5H PYROMETER.

When the oven reaches the desired temperature, the emissivity is adjusted on the pyrometer to obtain the same temperatures. Table 3.2 shows the emissivity and transmittance of a 16 vol% (Ni-Zn) ferrite-alumina composite at different temperatures.

	1000°C	1100°C	1200°C
Emissivity	0,945	0,968	0,953
Transmittance	1,0	1,0	1,0

TABLE 3-2. EMISSIVITY AND TRANSMITTANCE OF 16 VOL% (NI,ZN) FERRITE-ALUMINA COMPOSITE AT DIFFERENT TEMPERATURES.

Microwave sintering of the samples is carried out using a SiC susceptor. Without a susceptor, the composite absorbs few microwaves, and its temperature remains too low to allow any sintering. The sintering process used is therefore called microwave hybrid heating. Figure 3.4 shows the microwave device used for sintering.
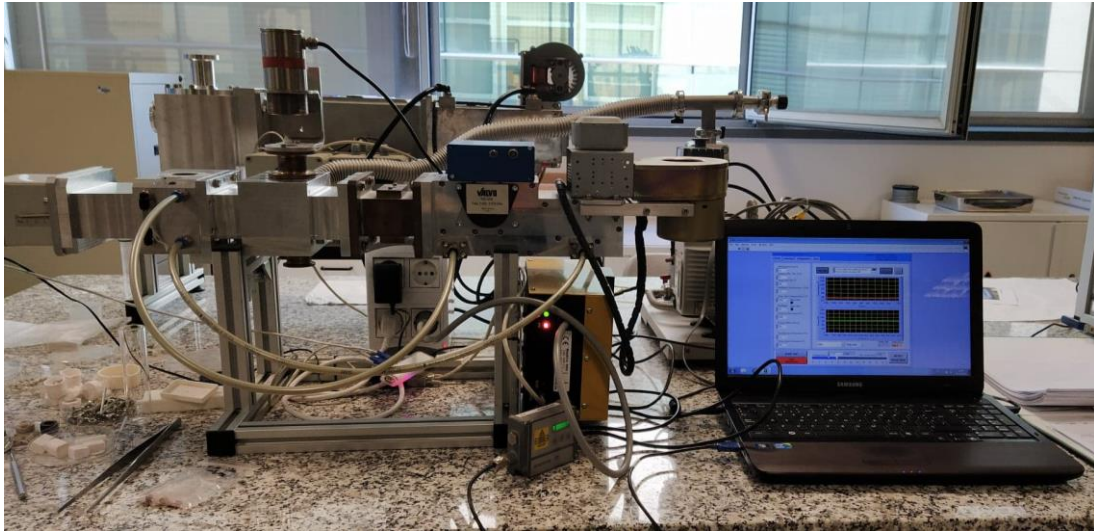
FIGURE 3-4. MICROWAVE EQUIPMENT.

During processing, the sintering of the Ni-Zn ferrite using magnetic microwaves was unsuccessful. Indeed, the material does not heat up enough to allow sintering. This may be related to the high electrical resistivity of Ni-Zn ferrite. As previously explained in this type of material the eddy current losses are very low. However, in the case of magnetic microwave sintering, eddy current losses are partly responsible for the increase in temperature of the material due to the Joule effect. This may therefore be an explanation for the issues encountered during sintering.

3.2.3 Cutting and embedding of the samples

The samples are cut in half so that they can be studied in their entirety and not just on the surface. In order to make precise cuts, the sample is glued to a base using a heated resin and then cut with a diamond wire, which makes small cuts at a slow speed. (Figure 3.5)

FIGURE 3-5. DIAMOND WIRE CUTTING MACHINE – MODEL 3242.

In order to measure their hardness and toughness, the samples must be embedded and polished. Half of the sample is then embedded in a transparent resin with a STRUERS brand machine (Figure 3.6). The powder containing the sample is first heated for 3.5 min at 180 °C and then cooled for 6 min at a pressure of 350 bar.
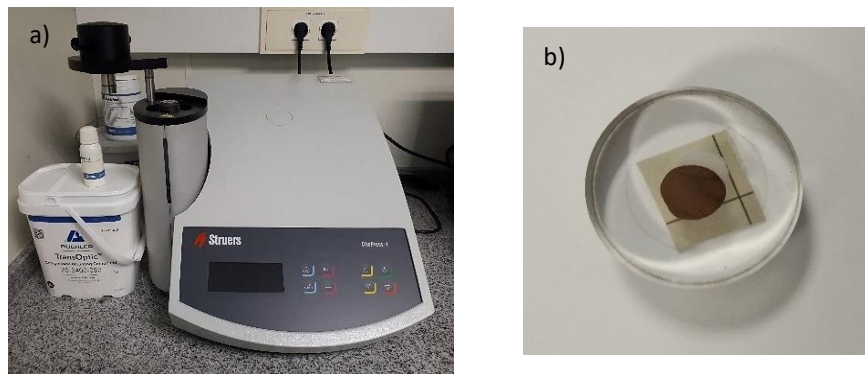
FIGURE 3-6. A) TRUERS EMBEDDING MACHINE AND B) SAMPLE IN THE RESIN.

3.2.4. Polishing

Finally, the samples are polished to a flat surface. Different polishing discs and lubricants are used for this purpose. Table 3.3 summarises the various polishing steps.

Grain	Lubricant	Load applied	Velocity	Time
75 µm	Water	10 N	100 rpm	5 min
40 µm	Water	10 N	100 rpm	1 min
20 µm	Water	10 N	100 rpm	1 min
10 µm	Water	10 N	100 rpm	1 min
MD Largo	6 µm	20 N	150 rpm	10 min
MD Plus	3 µm	20 N	150 rpm	8 min
MD Nap	1 µm + Oil	10 N	150 rpm	8 min

TABLE 3-3. POLISHING STEPS.

4) Characterization methods

4.1 Archimedes' density

The density of the samples is calculated using the Archimedes density method. The samples were first immersed in water and heated for 5 hours before remaining under water at room temperature for 20 hours.

The mass of the sample in the water was then determined using a balance equipped with a hydrostatic system (Figure 4.1). The samples were then dry in an oven for 2 hours. The mass of the sample was then measured.

FIGURE 4-1. BALANCE EQUIPPED WITH A HYDROSTATIC SYSTEM.

The density was measured using the following formula (Bella & Gremillard, 2016):

$$d = \frac{m_a}{V} = \frac{m_a}{m_a - m_e}$$ (4.1)

with V the volume of the sample, m_a the mass of the sample in air and m_e the mass of the sample in water.

4.2 Micro-hardness measurement

The hardness of a material is its resistance to plastic deformation in an indentation test. In this test, a given load is applied to the material using an indenter with a predefined geometry on a flat surface. Once the indenter is removed, the indentation left on the material is measured. (Güder, et al., 2011)

In this study the microhardness was determined using the Vickers indentation with a load of 9.8 N. The indenter in this case is a diamond pyramid with a square diamond base and an angle of 136° between the two opposite sides (Figure 4.2). (Smallman & Ngan, 2014) The Vickers microhardness HV is calculated with the following formula:

$$H_V[GPa] = \frac{2 \cdot F \cdot sin\frac{136°}{2}}{9,80665 \cdot d^2}$$

(4.2)

With *F* the load applied in *N* and d the average of the two indentation diagonal lengths d_1 and d_2 in mm.
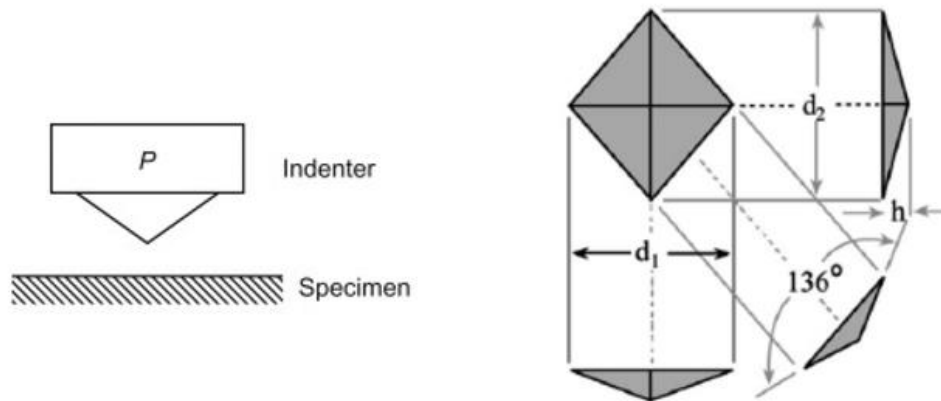
FIGURE 4-2. PRINCIPLE OF VICKERS MICRO-HARNESS MEASUREMENT.

The lengths of the diagonals were measured using an optical microscope. In order to have a significant hardness measurement, the test was performed 10 times on each sample.

4.3 Fracture toughness measurement

The toughness of a material is defined as its ability to resist crack propagation. Generally, in ceramics, crack propagation occurs according to mode I (opening mode). The K-factor represents the stress intensity in the region of the crack tip. (Ćorić, Ćurković, & Marijana Majić, July 2017) The fracture toughness is therefore called K_{IC} and represents the critical value of the stress intensity factor in mode I.

The fracture toughness was also measured by a Vickers indentation. The prints made for the Vickers hardness have been reused. There are two different crack profiles emanating from the Vickers indentation: radial-median and Palmqvist cracks. The type of crack generally depends on the load applied. Cracks formed at the four corners of the indentation are radial-median cracks if they develop an arc below the impression (Figure 4.3-a). On the contrary, if the cracks are only at the 4 corners of the indentation and not under the indentation, they are Palmqvist cracks (Figure 4.3-b).
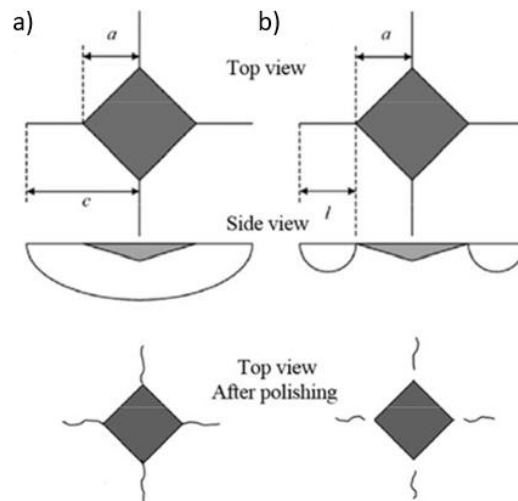
FIGURE 4-3. CRACKS FROM VICKERS INDENTATION: A) RADIAL-MEDIAN CRACK, B) PALMQVIST CRACK (ĆORIĆ, ĆURKOVIĆ, & MARIJANA MAJIĆ, JULY 2017).

If the ratio $\frac{c}{a}$ is less than 2,5, the material shows a Palmqvist crack. (Ćorić, Ćurković, & Marijana Majić, July 2017) In this case, to calculate the fracture toughness K_{IC}, the following formula proposed by Niihara is used.

$$K_{IC} = 0,0298 \cdot H_V \cdot a^{\frac{1}{2}} \cdot \left(\frac{E}{H_v}\right)^{\frac{1}{2}} \cdot \left(\frac{c}{a}\right)^{-1,38} \tag{4.3}$$

Otherwise, the material shows a radial-median crack. The fracture toughness K_{IC} is calculated with Evans' formula.

$$K_{IC} = 0,16 \cdot H_v \cdot a^{\frac{1}{2}} \cdot \left(\frac{c}{a}\right)^{-1,5} \tag{4.4}$$

For both of the formula, HV is the hardness of the sample in MPa, E the Young's modulus in MPa, *c* the crack length from the centre of the indentation to the crack tip in μm, and *a* the half of the indentation diagonal in μm.

All the measurements were made with an optical microscope and in order to have a significant value of fracture toughness, the measurements were performed 5 times for each sample.

4.4 X-ray diffraction (XRD)

X-ray diffractometry is a characterisation technique based on the diffraction of X-rays by matter that provides information about the spatial arrangement of atoms in a material. In the case of powder diffraction, the individual phases present can also be determined.

 A beam of monochromatic X-rays is projected onto the matter and is then reflected in specific directions according to Bragg's law (Figure 4.4). These rays will interfere with each other and create constructive or destructive interferences which cause maximum intensities in certain directions (Serna, Lagneau, & Carpentier, 2014). Interference is constructive if Bragg's law is equal to:

$$2 \cdot d \cdot \sin(\theta) = n \cdot \lambda \qquad\qquad (4.5)$$

with ϑ the half of the angle of deviation, λ the wavelength, d the inter-reticular distance (distance between two crystallographic planes) and n, an integer called the "diffraction order".
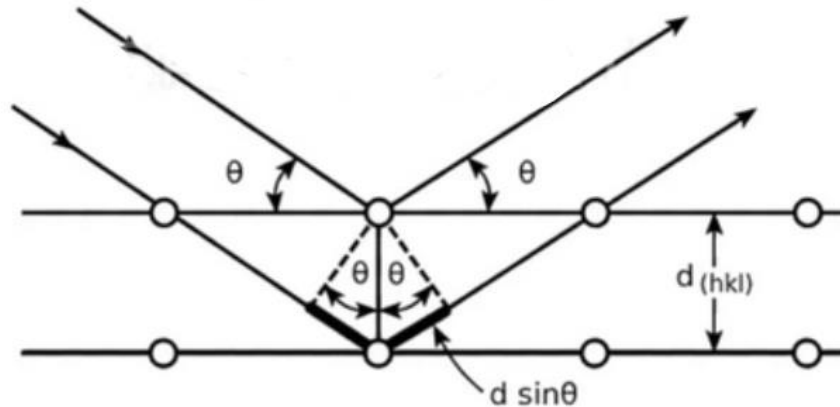
FIGURE 4-4. X-RAY BEAM INTERACTION WITH ATOMS AT INCIDENT ANGLE Θ (CRAVEN, 2019).

The intensities are recorded by sensors as a function of the deflection angles 2θ of the beam creating a graph called a diffractogram.

4.5 Scanning Electron Microscopy FE-SEM

FE-SEM is an electronical microscopy technique that uses the principle of electron-matter interaction to produce high-resolution images of the surface of a sample. A focalized electron beam is projected onto the material to be analysed and the electrons interact with the material. Different main signals are then emitted: secondary electrons, backscattered electrons, and X-rays. (Delvallee, 2014)

Secondary electrons are low-energy electrons (a few electron volts) emitted in the near-surface layers. These electrons will therefore be very sensitive to changes in the surface of the specimen and will thus make it possible to obtain a topographic contrast image. The backscattered electrons come from the interaction of the beam with the nuclei of the atoms and have a high energy (around 30 electron volts). They are sensitive to the atomic number of the target element and will therefore make it possible to distinguish phases with different chemical compositions. X-rays show the chemical composition and crystalline structure of the material. These emissions are picked up by specific sensors and will form an image with a resolution of the order of a nanometre.

A Field Emission (FE-SEM) is used to characterize the samples (Figure 4.5). A field emission gun is used as electron source which allows a highly focalized low and high energy beam to be formed, thus providing information with greater spatial resolution. (Chillagana Pilapanta, 2019)
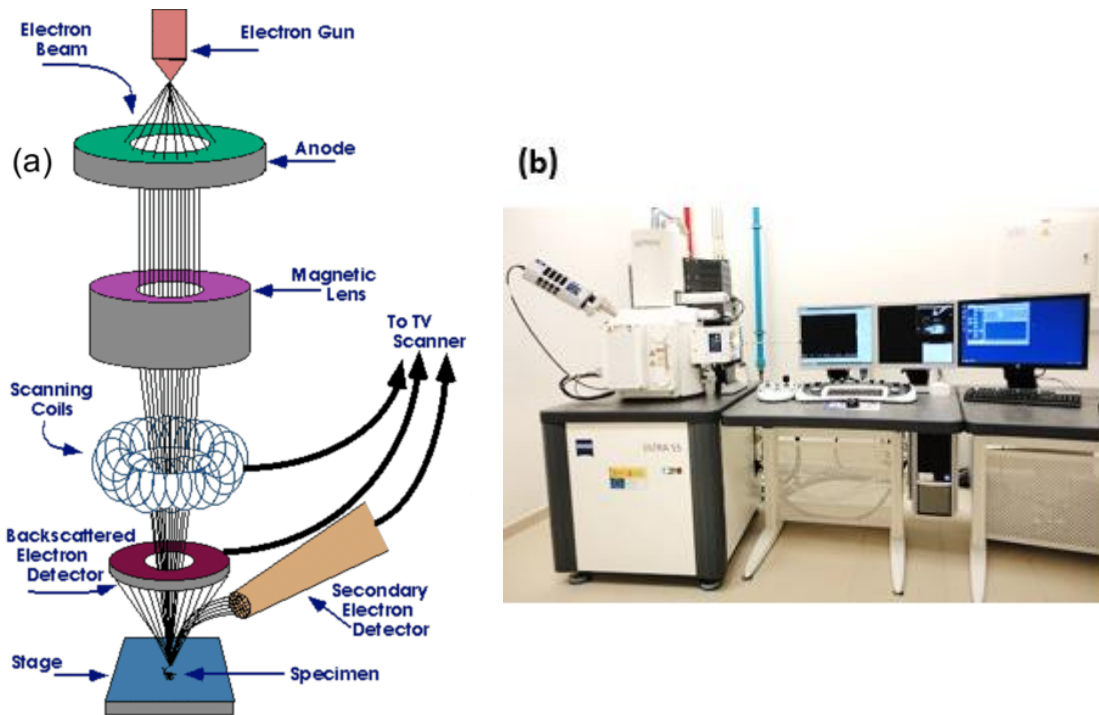
FIGURE 4-5. FE-SEM A) SCHEMA OF THE DEVICE, B) SEM USED: ZEISS - GEMINI ULTRA (CHILLAGANA PILAPANTA, 2019).

Based on the image obtained by FE-SEM, grain size has been measured with an image analysis program.

5) Results and discussion

Table 5.1 lists the various samples manufactured during this project.

Material	Sintering	Temperature	Time
16 vol% (Ni-Zn) ferrite-alumina	microwave	1000°C	10 min
		1100°C	10 min
		1200°C	10 min
	conventional	1100°C	1h
		1200°C	1h
		1200°C	2h
Alumina	conventional	1200°C	2h
		1300°C	2h
		1400°C	2h
(Ni-Zn) Ferrite	conventional	1250°C	2h

TABLE 5-1. SAMPLES MANUFACTURED BY CONVENTIONAL AND NON-CONVENTIONAL MICROWAVE SINTERING.

As a reminder, all samples manufactured by microwave sintering were made using a SiC susceptor.

5.1 Microstructure

5.1.1 XRD

In this section, the results obtained by XRD will be studied.

The initial powder of the composite Ni-Zn ferrite and alumina was first characterized.
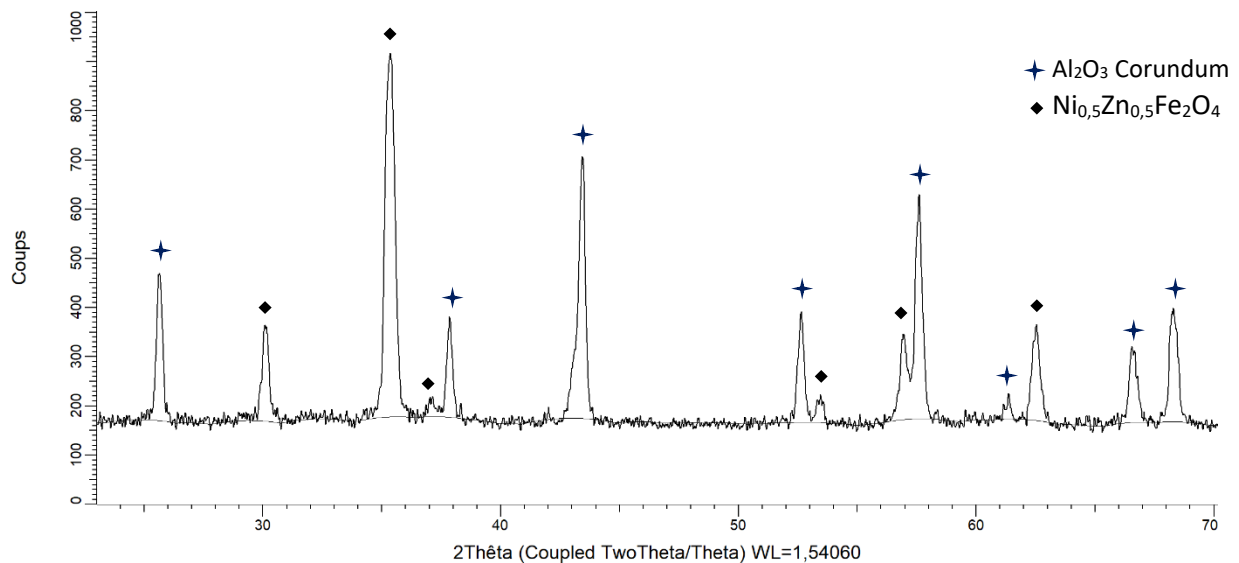
FIGURE 5-1. DIFFRACTOGRAM OF THE INITIAL POWDER.

The figure 5.1 shows the XRD diffractogram of the initial powder used for the sintering. Several peaks can be observed corresponding to alumina in its corundum form as well as Ni-Zn ferrite of the formula $Ni_{0,5}Zn_{0,5}Fe_2O_4$. The alumina has a hexagonal structure and the lattice parameter values found are close to the one given in the literature (Croquesel, 2015) with $a = 4.7582$ Å and $c = 12.9897$ Å. The Ni-Zn ferrite has a cubic structure.

The figure 5.2 below presents samples of the composite manufactured by conventional sintering at temperatures ranging from 1100 to 1200 °C for 1 or 2 hours. A shift among the spectra of the different samples of the composite is observed. This can be explained by the different temperatures used during sintering. As a matter of fact, such different thermal history can induce different thermal stresses, causing some distortion in the peaks in regard to the initial value. This phenomenon could also be explained by a thermal dilatation of the lattice, inducing a change in its parameter and so, a shift in the diffraction angle. It can also be seen that the characteristic peaks of the Ni-Zn ferrite are no longer present in the composite. The characteristic peaks of alumina are nonetheless still observable after sintering.

FIGURE 5-2. DIFFRACTOGRAM OF THE 16 VOL% (NI-ZN) FERRITE-ALUMINA COMPOSITE MANUFACTURED BY NON-CONVENTIONAL MICROWAVE SINTERING AT 1100°C (BLACK) DURING 1H AND 1200°C DURING 1H (RED) AND 2H (BLUE).

The new peaks seem to correspond to $Al_2Fe_2O_4$. The Ni-Zn ferrite has therefore reacted during conventional sintering and formed a new component. The absence of Zinc and Nickel in the diffractogram shows that their proportion in the final material is too small to appear. Hence, it is likely that these two elements have been dissolved in the material. Nonetheless, further investigations are required in order to define the actual cause of such phenomenon.

This reaction is also observed for samples of the composite synthesised by microwave sintering. The Figure 5.3 below represents samples of the composite synthetised by non-conventional microwave sintering at 1000, 1100 and 1200 °C for 10 minutes.
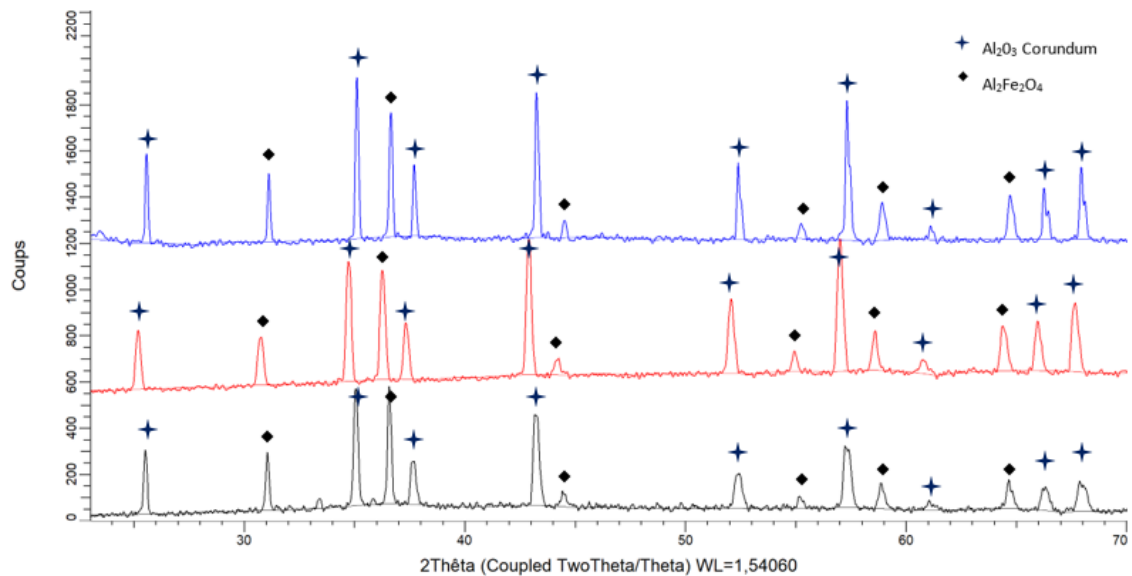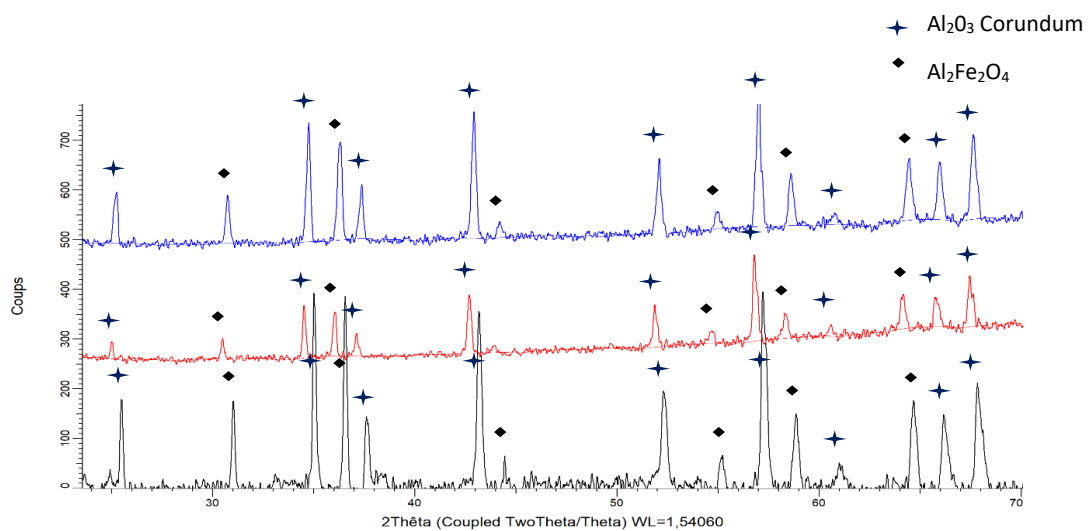

FIGURE 5-3. DIFFRACTOGRAM OF THE 16 VOL% (NI-ZN) FERRITE-ALUMINA COMPOSITE MANUFACTURED BY CONVENTIONAL SINTERING AT 1000°C (BLACK), 1100°C (RED) AND 1200°C (BLUE).

5.1.2 Density

As explained above, the densities of the samples were measured by the Archimedes density method.
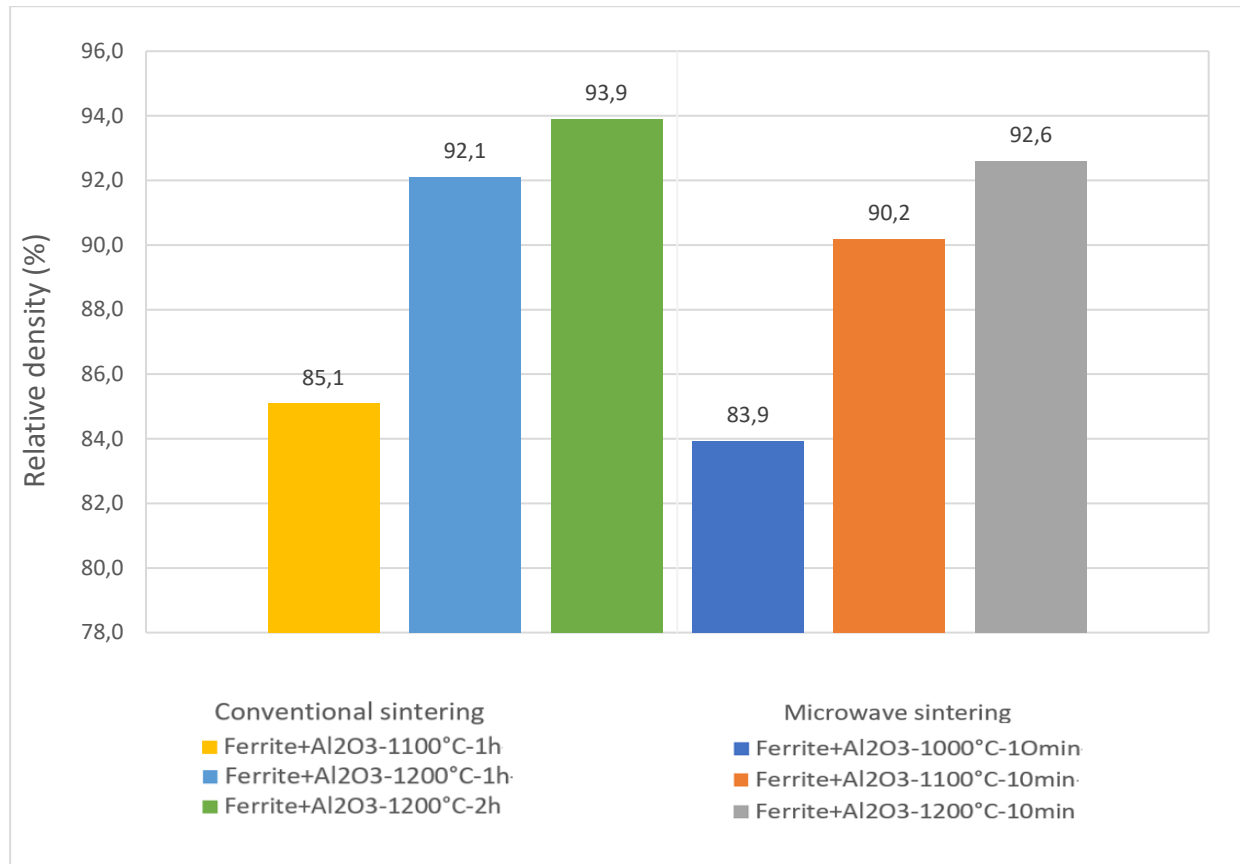
FIGURE 5-4. RELATIVE DENSITY OF THE 16 VOL% (NI-ZN) FERRITE-ALUMINA COMPOSITE MANUFACTURED BY CONVENTIONAL SINTERING AND NON-CONVENTIONAL MICROWAVES SINTERING.

Figure 5.4 is a histogram giving the relative density of each sample after its sintering. It can be seen that for the conventional sintering, the highest density is reached for the sample manufactured during 2 h under 1200 °C. As a matter of fact, a continuous densification of the part is observed with the increase of the temperature, as well as for a longer time of manufacturing. These results could suggest that the sintering is uniform and that no abnormal grain growth due to the temperature is observed for such process, or that this phenomenon is delayed under such conditions of manufacturing. The same phenomenon is observed with microwave sintering. Indeed, the density increases with the temperature.

Moreover, the density obtained by microwaves sintering is lower than the one obtained by conventional sintering for the composite. Conventional sintering at 1200 °C for 2 hour provides the highest density value. However, the 16 vol% (Ni-Zn) ferrite-alumina composite manufactured by microwave sintering for 10 minutes at 1200 °C has a density close to the one manufactured by conventional sintering at 1200 °C for 1 hour. For the same densification, the processing time is shorter. It would be interesting to manufacture the composite at higher temperature with microwave sintering in order to see if the densification continues to increase.

The same phenomenon is observed with the alumina manufactured by conventional sintering. The Figure 5.5 shows that the densification increases with the temperature.
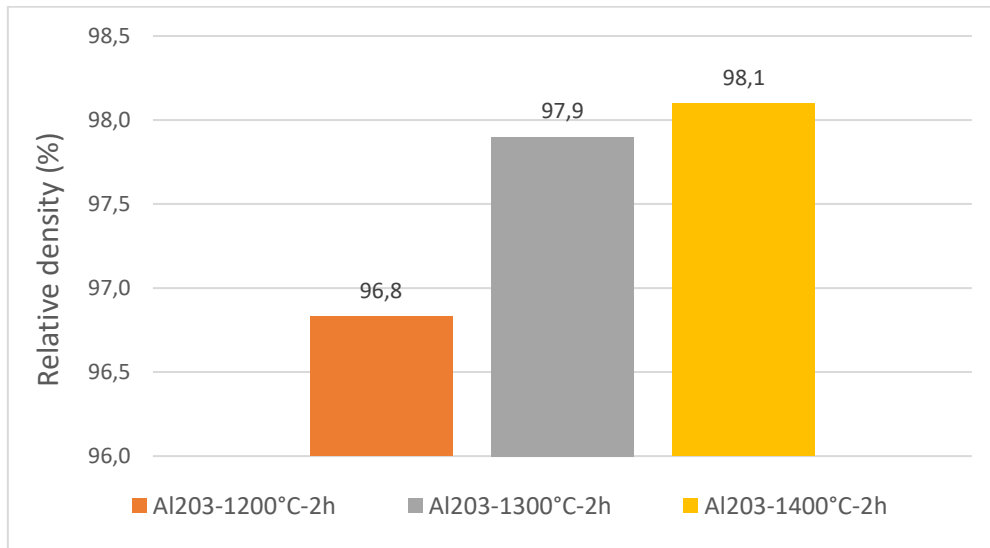
FIGURE 5-5. RELATIVE DENSITY OF THE ALUMINA MANUFACTURED BY CONVENTIONAL SINTERING.

5.1.3 FE-SEM

The samples were fractured, polished, and thermally attacked at 100 °C below the sintering temperature for 30 min. In this way the morphology and grain size can be seen.

Figure 5.6 shows FE-SEM photographs of the 16 vol% (Ni-Zn) ferrite-alumina composite manufactured by microwave sintering at different temperatures for 10 minutes.

FIGURE 5-6. FE-SEM PHOTOGRAPHS(X15) OF A 16 VOL% (NI-ZN) FERRITE-ALUMINA COMPOSITE MANUFACTURED BY MICROWAVE SINTERING AT A)1000°C, B)1100°C AND C)1200°C FOR 10 MINUTES.

At 1000 °C, the grains are still round and not really sintered. Many pores are also present. This temperature is therefore too low to allow the composite to be sintered. In addition, there is a phenomenon of abnormal grain growth characterised by the presence of large grains in the photograph. This phenomenon may be related to the presence of a secondary phase in the sample or to an anisotropy of the solid-solid surface tensions. The first hypothesis seems unlikely since the XRD does not show any secondary phase from the other samples. The samples at 1100°C and 1200 °C are at a more advanced stage of sintering. Indeed, the geometry of the grains have changed through their growth. At the same time, less porosities are observed.

Figure 5.7 shows FE-SEM images of the composite manufactured by conventional sintering at 1100 °C for 1 hour and 1200 °C for 1 and 2 hours. The 1100 °C picture shows numerous porosities and very small grains which are still very round in shape. Sintering is therefore not sufficient. At 1200 °C, the grain size is much larger, but many pores remain. The number of porosities decreases, and the grain size therefore increases with temperature.
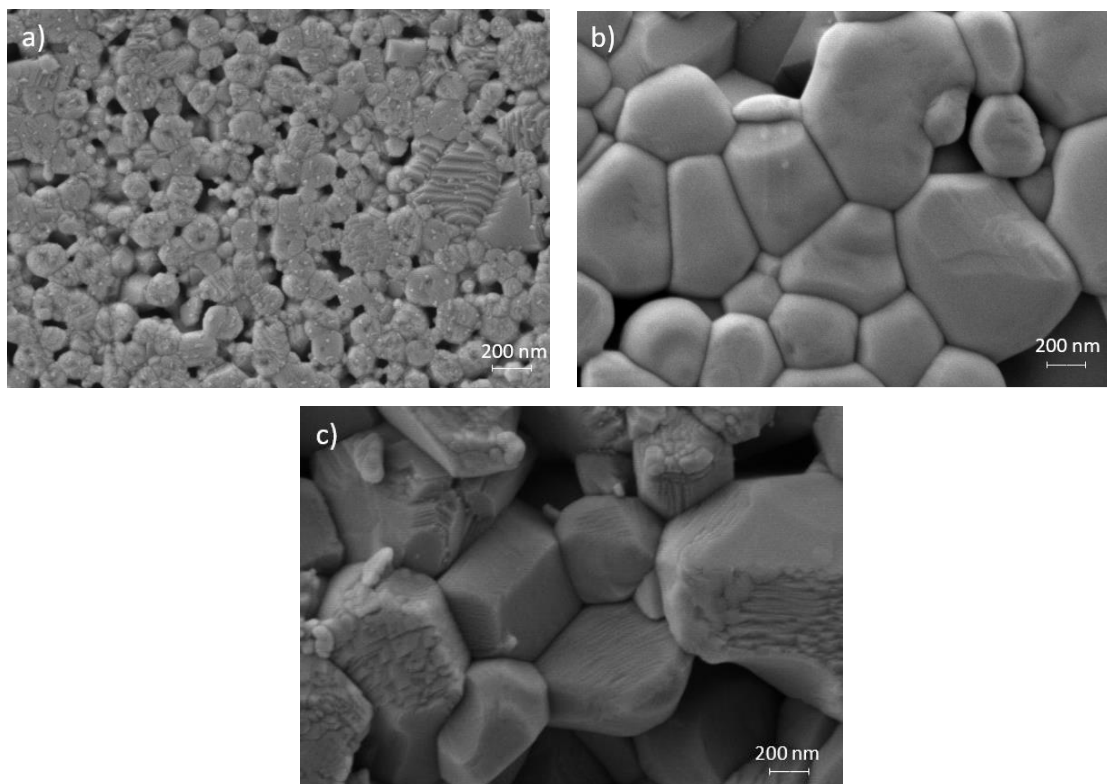
FIGURE 5-7. FE-SEM IMAGES (X40) OF A 16 VOL% (NI-ZN) FERRITE-ALUMINA COMPOSITE MANUFACTURED BY CONVENTIONAL SINTERING AT A)1100°C FOR 1H, B)1200°C FOR 1H AND C)1200°C FOR 2H.

By comparing the photographs obtained at 1100 °C and 1200 °C by conventional and microwave sintering, it can be seen that the porosity rate is lower in microwave sintering. Figure 5.8 shows that the grain size is bigger in microwave sintering than in conventional sintering at 1100 °C and tends to an equilibrium at 1200 °C. Microwave sintering therefore appears to allow faster grain growth and fewer pores than conventional sintering.
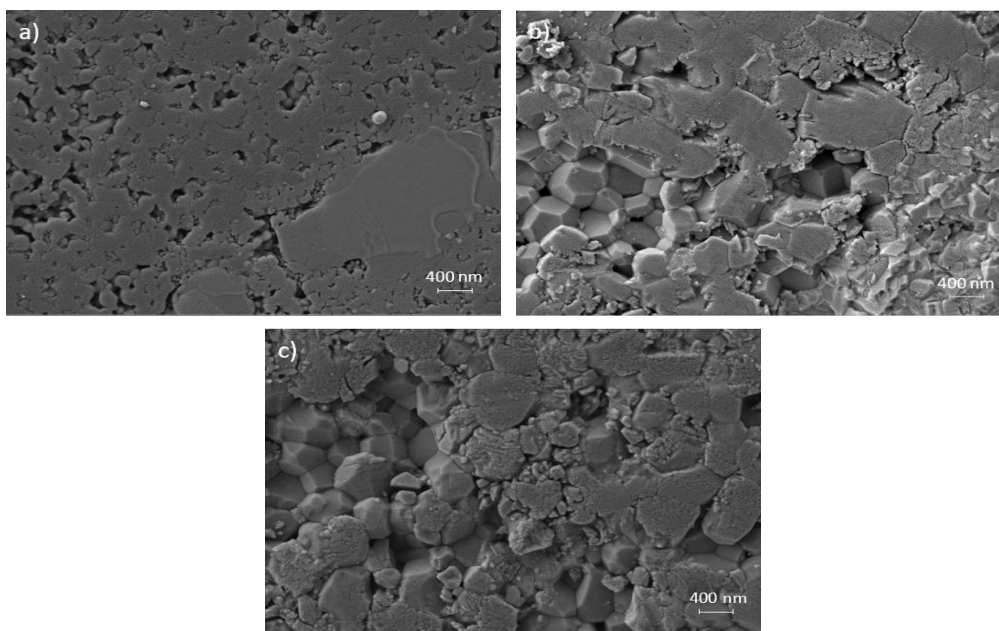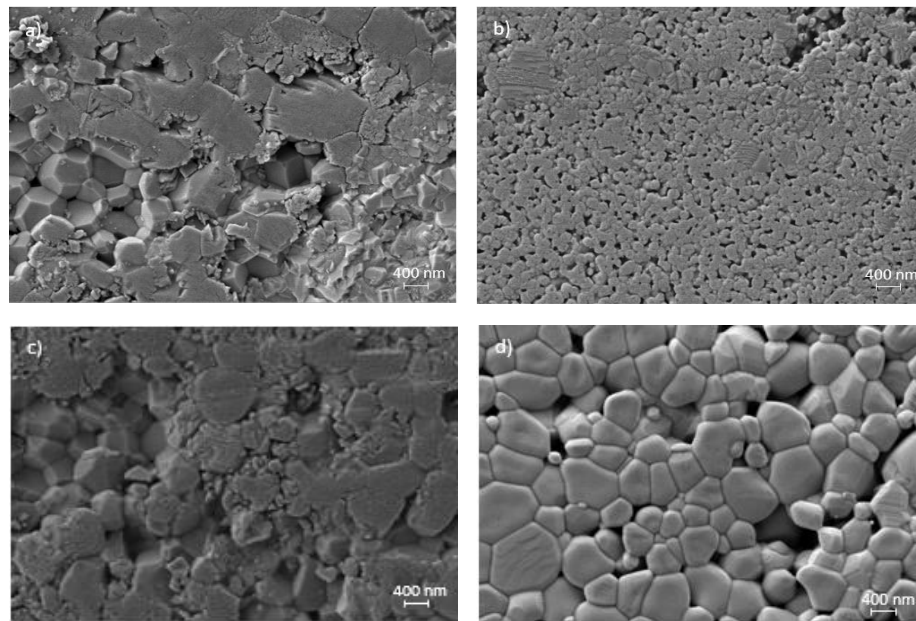
FIGURE 5-8. FE-SEM PHOTOGRAPHS(X15) OF A 16 VOL% (NI-ZN) FERRITE-ALUMINA COMPOSITE MANUFACTURED BY MICROWAVE SINTERING AT A)1100°C AND C)1200°C FOR 10 MINUTES AND BY CONVENTIONAL SINTERING AT B)1100°C AND C) 1200°C FOR 1H.

Finally, alumina samples were also studied at FE-SEM. Figure 5. shows FE-SEM images of alumina produced by conventional sintering at different temperatures for 2 hours. The sample at 1200 °C shows grains lacking cohesion, which is characteristic of a lack of sintering. The samples at 1300 °C and 1400 °C are only denser, although some porosities remain. This time again we observe that the number of porosities decreases, and the grain size increases with temperature.
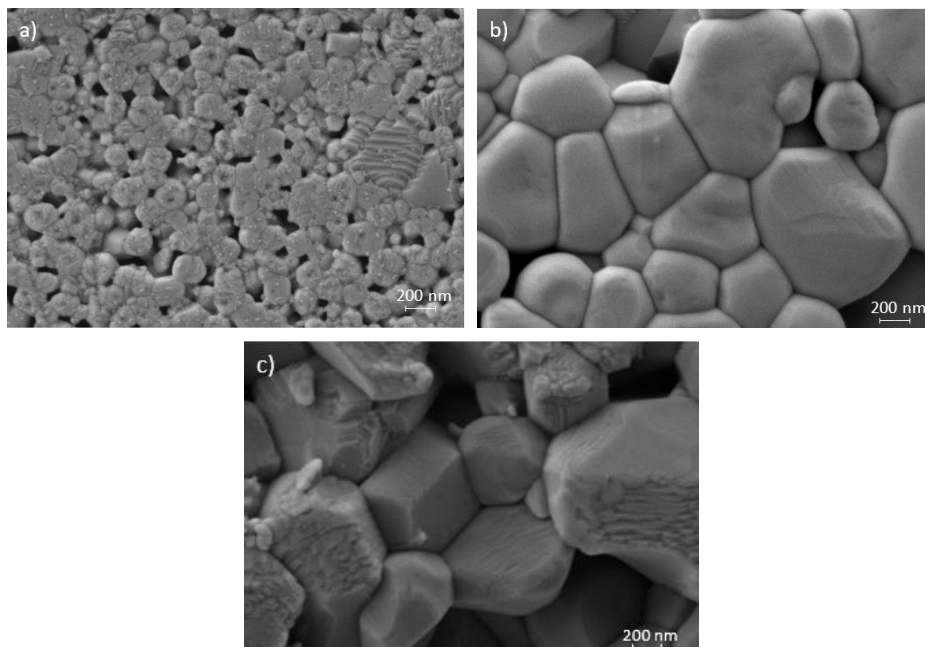
FIGURE 5-9. FE-SEM IMAGES (X40) OF ALUMINA OBTAINED BY CONVENTIONAL SINTERING AT A)1200 °C, B)1300 °C AND C)1400 °C FOR 2H.

5.2 Mechanical properties

5.2.1 Micro-hardness

Figure 5.10 shows the results of the microhardness tests on the composite samples. The measurements uncertainties are also present on the figure. Firstly, it can be observed that generally, the hardness of the samples obtained by microwave sintering is higher than that obtained by conventional sintering. Indeed, the specimen with the highest hardness is the one that has been sintered for 10 minutes at 1100 °C by microwave sintering. At 1200 °C, samples made by conventional sintering have a slightly lower hardness than those made by microwave sintering, but with a much longer processing time. Moreover, time of sintering does not seem to affect the hardness of the material, as it is shown by the samples manufactured at 1200 °C for 1 and 2 hours. Microwave sintering therefore achieves higher hardness with lower temperatures and shorter processing times than conventional sintering. No hardness values were found in the literature to compare with these values.
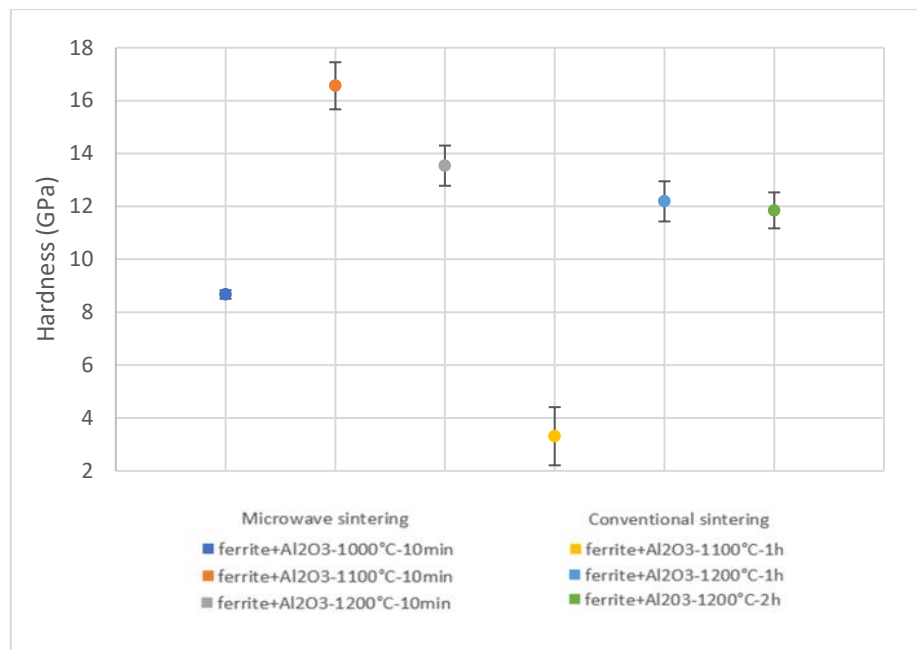
FIGURE 5-10. MICRO-HARDNESS OF THE 16 VOL% (NI-ZN) FERRITE-ALUMINA COMPOSITE MANUFACTURED BY CONVENTIONAL SINTERING AND NON-CONVENTIONAL MICROWAVES SINTERING.

Testing was also done on Ferrite-only samples in order to characterize their hardness. A sample of ferrite was manufactured by conventional sintering at 1250 °C for 2 hours. A Vickers hardness of 5,60 GPa was found. The composite has therefore a better hardness than the ferrite only.

Figure 5.11 shows that the hardness of alumina, sintered by conventional sintering. The results show that this value increases with the temperature. Indeed, the highest hardness is obtained at 1400 °C for 2 hours.
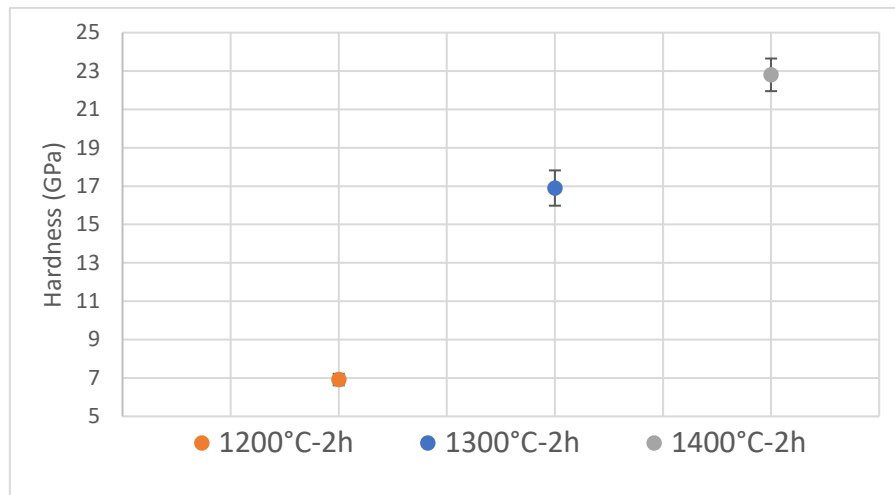
FIGURE 5-11. MICRO-HARDNESS OF ALUMINA MANUFACTURED BY CONVENTIONAL SINTERING.

5.2.2   Fracture Toughness

The results obtained in the tenacity tests will not be developed in this report. This because of some specimens which were not optimally sintered, so the material did not crack even when high loads were applied. In addition, the number of tests carried out was too small to obtain representative results. Due to the current health situation with COVID-19, access to the laboratory was restricted and therefore there was not enough time to carry out all the manipulations.

Also, the magnetic properties of the samples will not be developed in this report due to lack of access to the laboratory.

6) Conclusion

In this project, the main conclusions obtained are summarized below:

1) A 16 vol% (Ni-Zn) ferrite-alumina composite was produced by conventional (oven) and non-conventional microwave sintering using different durations and temperatures. The alumina was manufactured only by conventional sintering knowing that the material is transparent to microwaves. Ferrite was also manufactured by conventional sintering because the material did not heat up in contact with microwaves, preventing sintering from occurring.

2) Alumina sintered by conventional sintering has a linear behaviour. The higher the sintering temperature, harder the material is. The density follows the same trend.

3) XRD analysis shows that an unexpected phase reaction took place transforming $Ni_{0,5}Zn_{0,5}Fe_2O_4$ into $Al_2Fe_2O_4$ for both sintering processes.

4) The relative densities obtained are quite high, ranging from 83.9% to 93.9%. The highest density is reached for the sample manufactured for 2 h under 1200 °C by conventional sintering. Microwave sintering achieves slightly lower densities after 10 minutes This could have an economical interest.

As the density increases with temperature, it would be interesting to sinter further samples by microwave at temperatures above 1200 °C.

5) Regarding the hardness of the samples, the values are generally higher with microwave sintering process. As an illustration, the specimen with the highest hardness is the one that has been sintered for 10 minutes at 1100 °C by microwave sintering. This is quite interesting because microwave sintering uses shorter processing times.

7) Recommendation for further work

As in any research, there are still open questions and pending issues that require more detailed analysis or additional works.

The following actions will allow to complement the actual results:

- investigate why Ni-Zn ferrite does not rise in temperature under the effect of microwaves.
- investigate the origin of the phase transformation obtained during the sintering of the composite.
- study the electrical and magnetic properties of the samples.
- perform a high-resolution microscopy study in order to better characterise the microstructure.

8) Project budget

This part aims to establish the budget of the project.

8.1 Equipment

Initially, the price of equipment was taken into account. This equipment has a depreciation period of 10 years and as it was purchased a few years ago, it is considered that part of it has already been depreciated. Table 8.1 represents the upfront investment for the equipment used in the project. The price of the equipment is 262 225,00 €.

Equipment	Reference quantity	Price per unit (€)
Precision Balance and density measuring equipment	1	8 000,00
Cold isostatic pressing machine	1	10 000,00
Microwave sintering	1	50 000,00
Heating plate	1	325,00
Wire cutting machine Embedding machine Polishing machine with discs	1	63 000,00
Microhardness and computer equipment	1	22 900,00
Optical Microscope and computer equipment	1	80 000,00
Oven	1	28 000,00
Total		262 225,00

TABLE 8-1. PRICE OF THE EQUIPMENT.

8.2 Resources

This section lists the estimated costs of human resources (Table 8.2), laboratory tools (Table 8.3), reagents and products (Table 8.4), electrical power (Table 8.5) and laboratory technical services (Table 8.6) that were used during this project. Table 8.2 shows the cost of project labour. This price includes the time spent by the director for meetings, whether at the start of the project, during the bibliographical research or the experimental parts, as well as during the writing of the report. The hours spent by the laboratory technicians for the use of the equipment are also taken into account. Finally, the time spent by the materials engineer trainee during the bibliographical research, the manipulations and the report is also counted.

Person	Unity of measurement	Quantity
Project Director	h	54
Laboratory Technician	h	5
Student engineer	h	700

TABLE 8-2. HUMAN RESSOURCES.

Tool	Unity of measurement	Quantity
Beaker 100mL	Ud	6
Metal clamps	Ud	1
Metal spatula	Ud	1
Ceramic crucible	Ud	1
Latex glove box	Ud	1
Rubber ball packet	Ud	1

TABLE 8-3. LABORATORY TOOLS.

Material	Unity of measurement	Quantity
Alumina Taimei	g	50
Ni-Zn ferrite from Ferroxcube	g	50
Distilled water	mL	2000
Diamond paste abrasive	mL	500
Resin embedding	g	210

TABLE 8-4. REAGENTS AND PRODUCTS.

Equipment	Power (W)	Estimated hours of use (h)	Unity of measurement	Quantity
Precision balance	15,5	2	kW.h	0,03
Microwave sintering	800	5	kW.h	4,00
Heating plate	1020	5	kW.h	5,10
Wire cutting machine	750	6	kW.h	4,50
Embedding machine	1000	4	kW.h	4,00
Polishing machine	570	15	kW.h	8,55
Microhardness + Equipment	150	12	kW.h	1,80
Optical Microscope and computer equipment	320	10	kW.h	3,20
Oven	4500	15	kW.h	67,50
Total power consumption			kW.h	98,68

TABLE 8-5. ELECTRICAL ENERGY CONSUMPTION.

Services	Unity of measurement	Quantity
Electronic microscopy service of the Universidad Politècnica de València FE-SEM team. Including sample preparation material.	h	10
X-ray SCSI service. UPV agreement with UV. Phase identification.	sample	20

TABLE 8-6. LABORATORY TECHNICAL SERVICES.

8.3 Unit price tables

This section provides tables of unit prices for human resources (Table 7.7), laboratory tools (Table 7.8), reagents and products (Table 7.9), electrical energy (Table 7.10), and technical services (Table 7.11).

Person	Reference quantity	Price (€)	Unit price (€ ud^{-1})
Project Director	1	24,00	24,00
Laboratory Technician	1	12,30	12,30
Student engineer	1	12,50	12,50

TABLE 8-7. UNIT PRICE: HUMAN RESOURCES.

Tool	Reference quantity	Price (€)	Unit price (€ ud^{-1})
Beaker 100mL	1	0,96	0,96
Metal clamps	1	2,55	2,55
Metal spatula	1	2,89	2,89
Ceramic crucible	1	3,20	3,20
Latex glove box	1	4,39	4,39
Rubber ball packet	1	2,00	2,00

TABLE 8-8. UNIT PRICE: LABORATORY TOOLS.

Material	Reference quantity	Price (€)	Unit price (€ ud^{-1})
Milligram of Alumina Taimei	1000	134,20	0,134
Milligram of Ni-Zn ferrite from Ferroxcube	1000	120,90	0,121
Millilitre of distilled water	5000	10,92	0,002
Millilitre of diamond paste abrasive	1000	160	0,16
Milligram of resin embedding	2300	200	0,087

TABLE 8-9. UNIT PRICE: REAGENTS AND PRODUCTS.

	Reference quantity	Price (€)	Unit price (€ ud^{-1})
Kilowatt-hour	1	0,0855	0,0855

TABLE 8-10. UNIT PRICE: ELECTRICAL ENERGY.

	Reference quantity	Price (€)	Unit price (€ ud^{-1})
FE-SEM electron microscopy service hour, material included	1	20	20
X-ray diffractometry sample	1	8	8

TABLE 8-11. UNIT PRICE: TECHNICAL SERVICES.

8.4 Partial budget

Person	Unity	Unit price (€ ud⁻¹)	Cost (€)
Project director	54	2,.00	1296,00
Laboratory Technician	5	12,30	61,50
Student engineer	700	12,30	8750,00

TABLE 8-12. PARTIAL BUDGET: HUMAN RESOURCES.

Tool	Unity	Unit price (€ ud⁻¹)	Cost (€)
Beaker 100 mL	6	0,96	5,76
Metal clamps	1	2,55	2,55
Metal spatula	1	2,89	2,89
Ceramic crucible	3	3,20	9,60
Latex glove box	1	4,39	4,39
Rubber ball packet	1	2,00	2,00

TABLE 8-13. PARTIAL BUDGET: LABORATORY TOOLS.

Material	Unity	Unit price (€ ud⁻¹)	Cost (€)
Milligram of Alumina Taimei	50	0,134	6,7
Milligram of Ni-Zn ferrite from Ferroxcube	50	0,121	6,05
Millilitre of distilled water	2000	0,002	4,00
Millilitre of diamond paste abrasive	500	0,16	80,00
Milligram of resin embedding	210	0,087	18,27

TABLE 8-14. PARTIAL BUDGET: REAGENTS AND PRODUCTS.

	Unity	Unit price (€ ud⁻¹)	Cost (€)
Kilowatt - hour	98,68	0,0855	8,44

TABLE 8-15. PARTIAL BUDGET: ELECTRICAL ENERGY.

	Unity	Price (€)	Cost (€ ud⁻¹)
FE-SEM electron microscopy service hour, material included	10	20	200
X-ray diffractometry sample	20	8	160

TABLE 8-16. PARTIAL BUDGET: TECHNICAL SERVICES.

8.5 Total project budget

Table 7.17 shows the total estimated cost for this project. This estimation includes only those items for which the value is known.

Category	Cost (€)
Human resources	10 107,50
Equipment	262 252,19
Reagents and products	115,02
Electrical energy	8,44
Technical services	360
Total (without IVA)	272 843,15
IVA (21 %)	57 297,06
Total (IVA include**)**	330 140,21

TABLE **8-17. T**OTAL PROJECT BUDGET**.**

9) Bibliography

Ali, M. A., Khan, M. N., Chowdhury, F.-U.-Z., Akhter, S., & Uddin, M. M. (n.d.). Structural Properties, Impedance Spectroscopy and Dielectric Spin Relaxation of Ni-Zn Ferrite Synthesized by Double Sintering Technique.

Alvaro, P. B. (2016). *advanded ceramic materials for dental applications sintered by microwave heating.* Ph.D thesis , UPV, mechanical and materials engineering department, Valencia.

Bella, M. L., & Gremillard, L. (2016). Caractérisation de pastilles en céramiques des mitigeurs de robiners produits a setif. *5*(2).

Benavente, R., Borrell, A., Dolores Salvador, M., García-Moreno, O., Peñaranda-Foix, F. L., & Catalá-Civera, J. M. (2014). Fabricatio of near-zero thermal expansion of fully dense beta-eucryptite ceramics by microwave sintering. *40.*

Bernache-Assolant, D., & Bonnet, J.-P. (2005). *Frittage : aspects physico-chimiques - Partie 1 : Frittage en phase solide.* Mécanique | Travail des matériaux - Assemblage. Techniques de l'ingénieur.

Borrell Tomás, M. A., & Salvador Moya, M. D. (2018). *Materiales cerámicos avanzados: procesado y aplicaciones.* Valencia: Editorial Universitat Politècnica de València.

Borrell, A., Dolores Salvador, M., . Penaranda-Foix, F. L., & Catala-Civera, J. M. (2013). Microwave sintering of zirconia materials: Mechanical and microstructural properties. *10*(313-320).

Chillagana Pilapanta, P. A. (2019). *Proyecto de desarrollo de nuevos materiales compuestos base circona con adicion de MoSi2 para su uso a altas temperaturas.* Universitat Politècnica de València.

Ćorić, D., Ćurković, L., & Marijana Majić, R. (July 2017). Statistical analysis of vickers indentation fracture toughness of Y-TZP Ceramics.

Costaa, A., Tortellab, E., Morelli, M., & Kiminami, R. (2003). Synthesis, microstructure and magnetic properties of Ni-Zn ferrites. *256*, 174-182.

Craven, R. (2019, March 11). *Using X-Ray Diffraction to Determine Crystal Structure*. Consulté le November 2020, sur study.com.

Croquesel, J. (2015). *Etude des spécificités du frittage par micro-ondes de poudres d'alumine alpha et gamma.* Ph. D Thesis, Université Grenoble Alpes, Grenoble.

Delvallee, A. (2014). *Métrologie dimensionnelle de nanoparticules mesurées par AFM et par MEB.* ENSTA-PARISTECH.

Frajer, G. (2018). *Synthèses, mise en forme et étude des propriétés magnétiques de ferrites (NiZnCuCo)Fe2O4 en fréquence.* Ph. D Thesis, Science des matériaux [cond-mat.mtrl-sci]. Université Grenoble Alpes, Grenoble.

Güder, H., Sahin, E., Sahin, O., Göçmez, H., Duran, C., & Cetinkara, H. (2011). Vickers and Knoop Indentation Microhardness Study of β-SiAlON Ceramic. *120*(6).

Guyon, A. (2013). *Frittage ultra-rapide naturel : chauffage par micro-ondes et par induction.* Université de Grenoble.

Katz, J. (1992). Microwave sintering of ceramics. *22*(153-170).

Lapointe, P. (2010). *DÉVELOPPEMENT D'UN COMPOSITE MAGNÉTIQUE DOUX AVEC REVÊTEMENT DE FERRITE NANOMÉTRIQUE.* Ph. D Thesis, Département de génie des mines, de la métallurgie et des matériaux, faculté des sciences et de génie, université Laval, Québec.

Lebourgeois, R. (2005). *Ferrites doux pour l'électronique de puissance.* Institut national polytechnique de Grenoble. Techniques de l'Ingénieur.

Levin, I., & Brandon, D. (1998). Metastable Alumina Polymorphs: Crystal Structures and transition sequences. *81*(8).

Lorraine F, F. (2016). *Chapter 5 - Powder Processes.* Academic Press.

Mauss, F. (1994). *Étude de la décomposition thermique de l'alun d'ammonium.* Ecole Nationale Supérieure des Mines de Saint-Etienne.

Oghbaei, M., & Mirzaee, O. (2010). Microwave versus conventionnal sintering : a review of fundamentals, advantages and applications. *494 :175–189*.

Rahaman, M. (2007). *Sintering of ceramics (taken and modified).* CRC Press.

Sano, S., & Makino, Y. (2000). 30 and 83 GHz millimeter-wave sintering of alumina. *19*(2247-2250).

Serna, F., Lagneau, J., & Carpentier, J.-M. (2014). La diffraction des rayons X : une technique puissante pour résoudre certains problèmes industriels et technologiques. *116*.

Smallman, R., & Ngan, A. (2014). *Modern Physical Metallurgy (Eighth Edition).*

Sutton, W. (1992). Microwave processing of ceramics - an overview. *269*.

Yadoji, P., Peelamedu, R., Agrawal, D., & Roy, R. (2003). Microwave sintering of Ni-Zn ferrites : comparison with conventional sintering. *Materials Science and Engineering, 98*(3), pp. 269-278. doi:10.1016/S0921-5107(03)00063-1